Microstructure and Creep Behaviour of MRI230D Magnesium Alloy

Microstructure and Creep Behaviour of MRI230D Magnesium Alloy

A thesis submitted in partial fulfilment of the

requirements for the degree of

Master of Technology

in

Metallurgical and Materials Engineering

by

Arjun Rajiv Kesavan

Roll No: 212MM1337

Department of Metallurgical and Materials Engineering
National Institute of Technology, Rourkela
May 2014

Microstructure and Creep Behaviour of MRI230D Magnesium Alloy

A thesis submitted in partial fulfilment of the

requirements for the degree of

Master of Technology

in

Metallurgical and Materials Engineering

by

Arjun Rajiv Kesavan

Under the guidance of

Prof. Ashok Kumar Mondal

Department of Metallurgical and Materials Engineering
National Institute of Technology, Rourkela
May 2014

CERTIFICATE

This is to certify that the thesis entitled, "Microstructure and Creep Properties of MRI230D Magnesium Alloy" submitted by Arjun Rajiv Kesavan (212mm1337) in partial fulfillment of the requirements for the award of Master of Technology in Metallurgical and Materials Engineering at the National Institute of Technology, Rourkela is a bonafide research work carried out by him under my supervision and guidance.

To the best of my knowledge, the matter embodied in the thesis is based on candidate's own work, has not been submitted to any other university / institute for the award of any degree or diploma.

Date: **Supervisor**

Place:

Prof. Ashok Kumar Mondal
Dept. of Metallurgical and Materials Engg.
National Institute of Technology
Rourkela – 769008

ACKNOWLEDGEMENT

I take this opportunity to offer my sincere gratitude to the Department of Metallurgical and Materials Engineering, National Institute of Technology Rourkela for offering a platform to gain exposure and gather knowledge.

I wish to extend my honest and gratefulness to my supervisor Prof. A. K. Mondal, a true guide who supported and encouraged me during the entire tenure of the project. He inspired me to drive this thesis towards the path of accomplishment. I also thank Prof. B. C. Ray, Head of the Department, Department of Metallurgical and Materials Engineering, National Institute of Technology Rourkela for granting me permission to initiate the project and avail all the facilities in the department. I also express my gratitude to all other Professors of our department for their co-operation and valuable advice during the course work and my project work.

I am obliged technical assistants Mr. U. K Sahu and Mr. Thanthi for the support they rendered during the execution of my project. I will never forget to mention some of my seniors, Anil, Mohan and Shaibu who helped me with multiple ideas during completion of my thesis. Also I would like to thank my colleagues Ravi, Rishikesh, Sandeep, Lenin and Suvin for their support and assistance during multiple phases of the work.

There are many who I may have left out in the acknowledgement, but without which I would not have successfully completed this work for which I am deeply indebted to. Finally, I thank God almighty and my parents for the towering strength.

Date:

Place: Arjun Rajiv Kesavan

ABSTRACT

The dependency of creep behaviour on the as-cast microstructure of MRI230D Mg alloy produced by ingot casting (permanent mould casting) and high pressure die casting was investigated. A detailed microstructural characterisation and study of creep properties have been accomplished. The alloy in both ingot-casting (IC) and high pressure die-casting (HPDC) conditions consists of α-Mg, C36 ($(Mg,Al)_2Ca$) and Al-Mn rich phases. Microstructural study revealed finer grain size, closely spaced network and increased volume fraction of secondary eutectic phases for HPDC specimen when compared to that of the IC specimen. The grain size variation and denser network of eutectic phases was due to the considerable difference in cooling rate, high degree of undercooling associated with the faster cooling rate following HPDC facilitates the formation of a large number of nuclei in the liquid Mg alloy. The eutectic C36 phases were also observed to be coarser in the case of IC specimen owing to the slower solidification rate. Porosity was discovered significant in the HPDC specimen in comparison to the negligible extent in IC specimen.

Following creep tests at 70 MPa stress level and temperature of 175°C and 200°C the HPDC specimens exhibited superior creep resistance as compared to the IC specimens. The significant creep resistance exhibited by the HPDC specimen was primarily due to the dispersion strengthening effect offered by hindering of dislocation movement at the grain boundaries. Stress dependence on the strain rates for the alloys cast by both the technologies were studied and deduced that the dominant creep mechanism was dislocation creep. The same was theortically confirmed from the deformation mechanism map established for Mg alloys. Post creep microstructural studies revealed increased precipitation of C36 phase at the grain boundaries. Larger amount of precipitation was observed in the HPDC specimens due to enhanced pre-existing eutectic phases in the same.

LIST OF FIGURES

LIST OF TABLES

TABLE OF CONTENTS

CHAPTER 1: INTRODUCTION

1.1 Introduction

Customer satisfaction in luxury, performance and attractive safety features in the contemporary automobiles have led to a gradual increase in vehicle weight leading into increased fuel consumption and ultimately elevated CO_2 emissions [1]. Hence, the automotive industry is progressively looking for stronger and lightweight material replacements, in order to stay inside the emission regulations. Magnesium with a key advantage of low density plays a principal role in automobile industry to beat this issue. With a density that is approximately two-third that of aluminium, the potential weight saved from increased magnesium usage has significant environmental impact, with reduction of greenhouse gas emissions. In addition, magnesium also delivers solution for global environmental crisis like reusability and recyclability unlike polymers. High specific strength, dimensional accuracy, good machinability and casting properties are some of the key features. [2]

Powertrain components meant for elevated temperature sustainability are one of chief areas for researchers working with magnesium alloys. The biggest challenge was the inferior creep resistance beyond a temperature of 100°C owing to the existence of thermally unstable β-$Mg_{17}Al_{12}$ phase, an intermetallic produced along the grain boundaries[3]. Obviously, the $Mg_{17}Al_{12}$ phase makes it unsuitable for use in the temperature range of 150-275°C and 50-80 Mpa in the case of powertrain applications[4,5]. Minor alloying elelments like RE, Ca, Si, Sn, Sb etc. were introduced in order to produce thermally stable intermetallics. Amongst all these combinations, Ca containing Mg-Al based alloys were promising and cost effective [6,7]. MRI230D is such an alloy developed by Dead-Sea magnesium and Volkswagen for to widen their service and implement over the limitations faced by AZ91, one of the most popular Mg alloys. The MRI230D Mg alloy promises optimum performance upto 190°C [8] and the alloy gifts an intermetallic that is superior in thermally stability, namely $(Mg,Al)_2Ca$ phase.

Mg alloys are primarily preferred in as-cast condition and the casting technology used is a determining factor for the performance. Sand casting, squeeze casting, permanent mold casting, thixocasting and high pressure die-casting are some of the known casting technologies used in the industry [9,10]. Major casting parameters like the type of mold

coating, mold pre-heat, melt superheat; pour time, dwell period and ejection determine the casting quality. Even the minor factors such as the melt handling tools affect the microstructure of the alloy. Moreover, the resulting as-cast alloys microstructural features such as extent of porosity, grain size, morphology and volume fraction of intermetallic phases, extent of solute supersaturation as well as the dominant strengthening mechanism affects the high temperature deformation and mechanical behaviour. As a result, all of the above mentioned parameters could bring about an appreciable change in the final performance of the alloy by the right choice of the casting technology keeping cost in mind. Gutman reported the effectiveness of casting variables on creep strength and stated that precipitation of $Mg_{17}Al_{12}$ phase enhanced creep deformation resistance of permanent mold alloy. Spiragarelli et al. [11] investigated creep characteristics of AZ91 alloy fabricated by die-casting, ingot-casting and thixoforming, established that the nature of creep behaviour of the alloy rest on on grain size and intragranular precipitates interrelating with dislocation movement. Ferri et al. [12] observed the relation between cooling rates and mechanical properties of ZAXLa 05413 and an association between grain size and SDAS with enhanced mechanical behaviour.

In addition, Han et al. [13] declared that the nanoscale indentation creep characteristics of AC52 alloy improved with an increase in cooling rate. Kim et al. [14] observed that the die-cast alloy having higher volume content of secondary phases showcased enhanced creep resistance as compared to the ingot-cast alloy in the Mg-4Al-2Sn-Ca alloy. Consequently, solidification rate and forcing of the melt along with mold properties that vary with different casting technologies affect the creep and mechanical properties. Creep behaviour is of prime focus in this work and understands the microstructural features that lead to the current behaviour.

1.2 Objective of the present work

In the present investigation, the need of studying further the inter-relationship of two different casting technologies at elevated temperatures, hence as-cast microstructure against the subsequent creep behaviour has been addressed. The comparison between high pressure die cast (HPDC) and ingot-cast (IC) products of MRI230D Mg alloy is studied with respect to the microstructural changes and resulting creep behaviour. This study is expected to help in the authentication for the better choice in mass production of powertrain components.

CHAPTER 2: LITERATURE REVIEW

This chapter studies the literature most relevant to the objectives of the thesis. The background and review is comprised of four parts. Part 1 offers a brief summary of the introduction to elemental magnesium, physical metallurgy, uses of magnesium and its alloys, a brief explanation on magnesium alloy naming conventions, discussion of Mg-Al-Ca alloys and the MRI230D alloy probed in this investigation. Part 2 reviews the processing routes (permanent mould cast/ingot cast and high pressure die cast) and the most important casting parameters. Part 3 consists of a condensed explanation of different creep mechanisms. Part 4 consists of a short description on the most relevant works that stood as the motivation for the present investigation of MRI230D alloy.

2.1 Magnesium and its alloys

2.1.1 Introduction to magnesium and its physical metallurgy

Magnesium is capable of offering revolutionary changes in various industries owing to its promising inherent properties. It could be seen as a possible replacement for many light metals and plastics that are ruling the automobile, electronic, aerospace, nuclear and domestic industries at present. This transformation shall occur if the alloy development in magnesium is scientifically routed for specific utility, though there are limitations in the application of magnesium.

Sir Humphrey Davy, a British chemist in 1808 first separated magnesium by consuming wet magnesium sulphate inside a voltaic electrolytic cell by means of a mercury cathode [15]. Pure elemental magnesium exposes high reactivity to oxygen and water since it possesses two valence electrons and an electrode potential equal to -2.375V [16]. If left without protection, magnesium fosters a hydroxide film [2] which makes it vulnerable towards oxidation unlike aluminium. Earlier usage was scarce due to immense reactivity of magnesium made it applicable only in powder and ribbon purposes for pyrotechnical applications. It was with the World War I and II and the initiation of the aviation and missile productions that the use of magnesium and the study of developing alloys originated.

Magnesium grows to a hexagonal close packed structure (HCP), Fig. 1, having lattice parameters of a = 0.3209 nm and c = 0.5211 nm (c/a = 1.624 being close to the ideal value of a HCP structure 1.633 [15]. The a and c lattice parameters increase with higher temperature, and the change in lattice space from room temperature to 597 °C for the a and c lattice parameter is stated to be 0.00573 nm and 0.00962 nm, respectively and c/a at 597°C is 1.62458 [15]. Aluminium has a bond length of nearly 286 pm and calcium reports 394 pm when magnesium reports 320 pm [17]. Hence alloying additions of aluminium minimises the parameters, increases the c/a ratio, while Ca addition increases it. The most attractive feature is its density, 1.745 g/cm^3 which is almost two thirds that of aluminium. Table 1 shows the atomic bond length of some common alloying additions in Mg alloys.

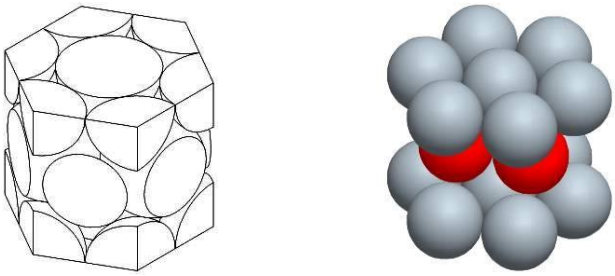

Fig. 1. Hexagonal close packed structure, unit cell (HCP), drawn to scale.

2.1.2 Magnesium alloy designation

The syntax of naming magnesium alloys is based on an alpha-numeric designation system, Table 2.3. For example, the Mg alloy AC52 has a nominal composition of Mg – 5 Al – 2 Ca (by wt. %). A concise description is provided in Table 4 and Table 5 contains two commercial alloys out of which one is the selected alloy (MRI230D) for this thesis work. However, MRI230D do not follow the conventional naming system.

Table 1. Alloy nomenclature convention of alphabetical symbols and elemental addition

Designation	A	E	H	J	K	M	Q	S	T	W	X	Z
Element	Al	Rare Earths	Th	Sr	Zr	Mn	Ag	Si	Sn	Y	Ca	Zn

Table 2. Two alloy compositions (wt %) developed by Dead Sea Magnesium Ltd. [19]

Alloy	Mg	Al	Ca	Mn	Sr	Zn	Sn
MRI230D	Bal	6.45	2.25	0.27	0.25	<0.01	0.84
MRI153M	Bal	7.95	0.98	0.20	0.27	<0.01	<0.01

2.1.3 Mg-Al-Ca alloys

Mg-Al-Ca alloys were established among the many other popular systems for their improved creep resistance, die-castability and realistic cost for vehicle powertrain applications. Alloys centred on the Mg-Al-Ca combination have been in application for several powertrain parts [20]. This genre of Mg alloy exhibit promising characteristics as research on fabrication and creep strengthening mechanisms moves ahead.

Al is the most widely used alloying element to magnesium alloys owing to its enhanced fluidity gifting the alloy. In addition, aluminium has appreciable solid solubility and castability in magnesium [21]. Al shows a maximum solubility in Mg at 437°C (eutectic temperature) of around l2.7% [22]. Al addition results in an increase in yield strength, whereas increase in UTS up to 6% and decrease followed by further addition are tsupprehe noticeable characteristics. However, the ductility increases initially up to 3% of Al addition and then decreases considerably. The solid solubility of aluminum in magnesium at room temperature is around 2%. Hence the excess Al forms $Mg_{17}Al_{12}$ intermetallic with Mg. This phase is hard, brittle and hence, acts as a strengthening structure at room temperature. However, Al also increases the possibility for shrinkage micro porosity up to 9% and then

reduces it [23]. It has also reported peak porosity at 9%. Aluminum also supports in corrosion resistance of Mg-Al alloys.

Investigations on addition of calcium in Mg alloys [24] reported that calcium appreciably enhanced the creep resistance of magnesium alloys. Inferior die casting characteristics like hot tearing, cracking, die sticking etc were testified, most importantly for Ca additions over 0.5 wt%. Sohn et al. [25,26] stated progressive enhancements in creep of AM50 with Ca additions from 0.25 - 0.88 wt%, particularly at high temperatures (150-200 °C), whereas retaining the ability to die cast the alloys. Powell et al. [27-29] die-cast a succession of alloys having high levels of Ca (1.8-3.1 wt. %) with a minimal Al amount of 5 wt. %. Unexpectedly at these comparatively high Ca content, the alloys were not exposed to the earlier testified hot cracking/die soldering and held the enhanced creep properties. Terada et al. [30], fruitfully cast a Mg-5 Al-1.72 Ca alloy with outcomes comparable to that of Powell et al. [27-29].

The studies on Mg-Al-Ca reported a microstructure having a primary α-Mg solid solution phase bounded by intermetallics at the grain boundary regions. Fig. 2 displays the die-cast and permanent mold-cast micrographs of AXJ530 Mg alloy. Pekguleryuz et al. [31], Sohn et al [25], and Lou et al. [27], all testified an Al_2Ca (or $(Mg,Al)_2Ca$ intermetallic, with progressively (with respect to the registered order of publications) advanced levels of investigations (EDS, X-Ray diffraction, and TEM diffraction, respectively) to attain this result. In addition, Ca completely repressed the crystallization of the intermetallic β phase, $Mg_{17}Al_{12}$. It was hence suggested that this high temperature phase Al_2Ca fully repressed the formation of the low temperature $Mg_{17}Al_{12}$ phase resultant [31], as being the key component for alloy strengthening at 150 °C along the interdentritic region.Sohn et al [25] also suggested that an increase in volume fraction of the Al_2Ca phase was seen with increased Ca content, hence reflected in the creep behaviour positively. Lou et al. [84] too testified the hexagonal $(Mg,Al)_2Ca$ which was thermally more stable to that of $Mg_{17}Al_{12}$ and having a coherent boundary with the α-Mg phase. They claimed that the $(Mg,Al)_2Ca$ phase was operative on pinning effect at the interdentritic zones, therefore elevating the general creep resistance.

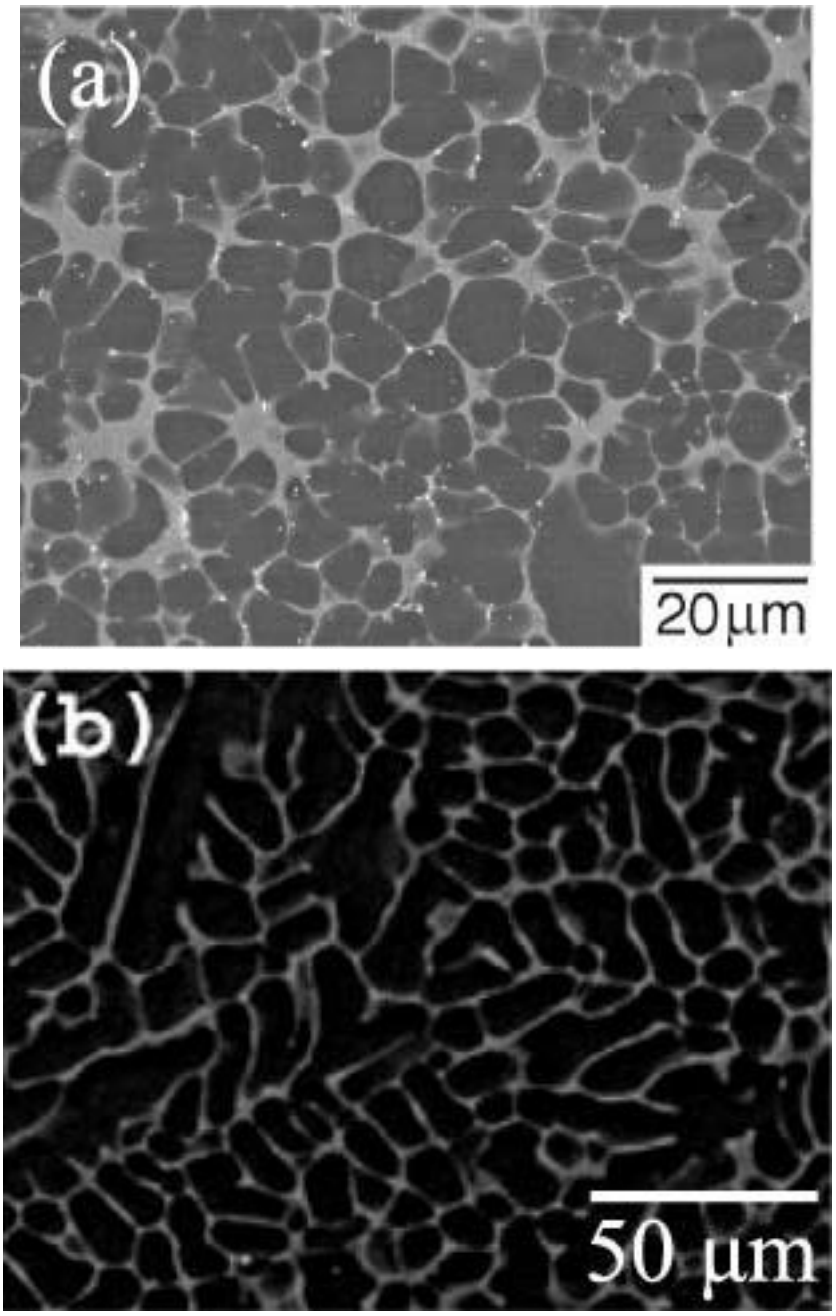

Fig. 2. Shows SEM micrographs of Mg-Al-Ca alloy (AXJ530), (a) Die-cast specimen and (b) Permanent mould cast specimen. [27].

Further studies done by Suzuki et al. [32-34] demonstrated various characteristics. The C36 intermetallic disintegrated to C14 (Mg_2Ca) and C15 (Al_2Ca) at 673 K (400 °C) and below, while thermally steady until 773 K (500°C). The working temperature of powertrain components being high, the decomposition of C36 is reported as slow.

A comprehensive study of creep properties of calcium-containing Mg alloys have been implemeted [27-29, 34, 35, 36-42]. Several investigations concluded operative creep mechanisms by finding the stress exponent from experimental outcomes (provided the validity of a power law creep expression holds good). Terada et al. [30] investigated die-cast Mg - 5% Al – 0.29% Mn – 1.72% Ca alloy with respect to its creep behaviour. The stress exponent between the temperature regime of 150 – 225 °C was testified to be n = 10. The computed activation energy needed for creep at the corresponding temperatures was Q_c = 142 kJ/mol, quantitatively close enough to the activation energy for magnesium self-diffusion. From the standard power law creep model, the values indicated the governing creep mechanism to be dislocation climb across α-Mg grain interior [30]. Hence the stress component and the stress component and Qc value determines the dominant creep mechanisms using the classic power law.

Lou et al. et al. [27-29] investigated the outcomes of calcium with micro alloyed Sr, less than 0.20 wt.%, on die-cast Mg-Al alloys. The stress exponent (n=1.5), 175 °C and stresses lower than 70 MPa) proved that grain boundary sliding determined the creep resistance, whereas at stresses higher than (>70 MPa, n=8.5) creep was urged by dislocation controlled climb and glide. In addition, the worthiness of the formation of the intermetallic $(Mg,Al)_2Ca$ was better understood and enhanced creep resistance. Along the matrix interior of Mg-3 wt.% Ca-5 wt.% Al-0.15 wt.% Sr alloys, the greatest resistance to creep was displayed. However, the part of the Sr addition on the creep resistance was not comprehended.

Sohn et al. [25, 26] investigated the compressive creep, of die-cast AM50 with Ca content between 0.25 and 0.88 wt.%. They stated a stress exponent of 6-9 at stresses going from 40-70 MPa and 150 °C. It was testified that calcium had no appreciable impact on the stress exponent. The enhancement in creep behaviour by the Ca additions was credited to the microstructural change at the grain boundaries (intermetallics).

Suzuki, et al. [35], investigated the influence of precipitation strengthening upon die-cast AXJ530 and reported enhancement of the creep rate by an order of 2-5 times of that examined

in an as-cast sample. As a whole, Mg-Al-Ca has proven by all means to be a promising combination if optimised to the required utility standards, they could deliver cost effective and industry specified performance.

2.1.4 MRI230D alloy

Table 6. shows the nominal chemical composition of the creep resisitant alloy invented by Dead Sea Magnesium Limited. The alloy promises creep deformation behaviour until 190°C. It is one of the most popular Mg-Al-Ca-Sr-Sn based alloys that are applied to the automobile industry. Following are the fundamental properties of the alloy:

Table 3. General mechanical properties of creep resistant MRI230D alloy [43]

Properties	**MRI230D**
Tensile yield strength [MPa]	
20°C	180
150°C	150
Ultimate tensile strength [MPa]	
20°C	245
150°C	205
Compression yield strength	180
Elongation in 50mm [%]	5
Impact strength [J]	6
Young's Modulus [GPa]	45
Fatigue strength [Mpa]	103
Creep Strength: Stress to produce 0.2% strain in 100 hr at 150°C [MPa]	15
Density at 20°C [g/cm^3]	1.8

2.1.5 Applications in automobile industry

The most exceptional features of magnesium are based on its inherent properties. Table 2, lists some of the key features of magnesium alloys that make them alluring to automotive, aerospace and other industries. Light weight feature is the most significant among these. High strength to weight ratio leads to relatively high specific stiffness and specific strength for magnesium alloys. Another very important advantage is the castability and dimensional

stability. Typical magnesium die-casting alloys such as AZ9lD, MRI230D, MRI153M, AM50A, MRI202S and AM60B can be cast into large and complex shapes with thinner sections. In addition, large die cast components those otherwise are made from assembling separately smaller cast sub components could be manufactured in a single–shot die casting.

Table 4. Advantages of magnesium alloys [18]

1	Light weight
2	Strength/Weight ratio
3	Excellent damping capacity
4	Non-magnetic, EMF shielding
5	Good heat dissipation
6	High castability
7	Complex and thin walled castings
8	Excellent machinability

Weight reduction being made the top priority without compromising the performance has led to the invention of many light alloys such as magnesium based alloys. The average size of the automobile has been steadily increasing with increased demand of facilities. Automobile industries are the most predominant beneficiary of magnesium research. Table 3 portrays most of the major applications of magnesium that are currently being addressed by the automotive industry. As the automotive industry struggles to reduce emissions and considerably improve fuel efficiency, the power train is an essential sector for development. It comprises of engine, the clutch, the transmission, the various drive shafts and the differential. The other competitors for the same automobile market are high performance plastics.

Table 5. Applications for magnesium alloys in the automotive industry.

	Component		**Product**
Inner	Airbag housing	Body	Door frame (Inner)
	Window regulator housing		Hatchback frame
	Glove box		Spare tyre jack
Chassis	Wheel	Powertrain	Automatic transmission case
	Control arm		Engine block, engine mount
	Rack and pinion housing		Crankcase
	Bracket for rail frames		Oil pan, oil pump housing
	Spare tyre rim		Starter housing

2.2 Casting Processes

The selection of a particular casting technology depends upon several factors such as the prerequisite number of castings, the essential properties, dimensions and contour of the component and the alloy castabiltiy [44]. While pressure die casting is widely used to produce many of the intricate parts, other casting technologies such as the gravity and low pressure castings via sand and permanent moulds are also popular. Investment casting process has also nowadays become popular in fabricating Mg alloy parts. Mg-Al and Mg-Al-Zn combinations also make use of gravity casting and sand casting process. Magnesium alloys having RE major alloying element are fabricated in sand casting route and implemented in aerospace applications. Furthermore, production is well advanced with squeeze casting and semi-solid processing like rheo casting and thixo casting. Out of the whole lot of advanced fabrication routes, high pressure die casting and permanent mould casting are the areas of concentration in this thesis work.

2.2.1 Permanent mould casting

Fig. 3, illustrates the permanent mold casting process. In the permanent-mold casting procedure, also called hard-mold casting, two halves of molds are made from materials such as cast iron, steel, bronze, graphite, or refractory metal alloys. The mold cavity and gating system consist of the mold. Gray cast iron isis one of the most commonly used mold material, especially large molds .The surface of the mold are coated with a refractory slurry (example; sodium silicate and clay) or sprayed with graphite for very few castings. The molds are held together by means of clamps and given a pre-heat of 150°C to 200°C and molten metal is poured down the sprue. For better solidification, fins are used. Permanent mold castings are not economical for small production runs, and sice removal from the mold casvity is difficult, complex shapes cannot be cast. However, if compared to sand casting, there are many benefits of the permanent mold casting such as surface finish, dimensional stability and enhanced mechanical properties due to faster solidification.

2.2.2 Die casting

The die-casting process is a further example of permanent mold casting, with the molten metal being forced into the die cavity at pressures ranging from 0.7MPa – 700MPa.The weight of most die-cast parts range from less than 90g to about 25 Kg. Die-casting is classified into two main methods namely; hot chamber die-casting and cold-chamber die casting. The fundamental difference between the two methods is that in cold chamber, the injection cylinder into which the metal is poured remains cold and in hot chamber, they are preheated. The casting process implemented in the present investigation is high pressure cold chamber die-casting.

The cold chamber die casting process is displayed in Fig. 4 [45]. The molten magnesium is supplied into a shot cylinder using hand ladling, auto-ladling, or by means of a pump. After that, the melt is injected (5-10 m/s) by a plunger inside cavity, there it gets solidified into the net shape component withstanding a high pressure (35-140 MPa). Finally, the cast material is ejected, and the part is sent for trimming.

The total cycle takes generally about 1 min. The contact time available for the molten magnesium in contact with the dies is greatly controlled by the short cycle time, almost avoiding the reaction with air or the die material. The sudden solidification (100-500°C/s based on cross section) end up with very fine grains particularly in the skins. High pressure

die casting (HPDC) presents convincingly flexible design possibilities and fabrication of light metals parts. The excellent die filling characteristics of magnesium alloys permit huge, thin-walled and complex castings to be produced economically by die-casting process, substituting steel structures that consist of several stampings and weldments.

GM (General Motors) took confidence in investing in the magnesium die casting technology and implemented its first high volume, one-piece die-cast instrument panel (IP) beam for magnesium in 1996[46]. In addition, a 12.3-kg component with nominal thickness of 4 mm, then the world's biggest magnesium die casting, gave a 32% mass reduction as that to the steel design and substantial performance enhancements (enhanced crashworthiness and decreased vibration) and cost reduction due to parts consolidation (25 parts in the magnesium design vs. 67 parts in steel)[47].

2.2.3 Casting parameters

Inspite of the similarities in the casting methods, some processes may better align closer to the specified application, depending on the property demands, casting size, production rate and design complexity .mold coating. The parameters that largely vary the resulting cast performance are many. Mold pre-heat, melt superheat, pouring time, dwell time and part ejection.

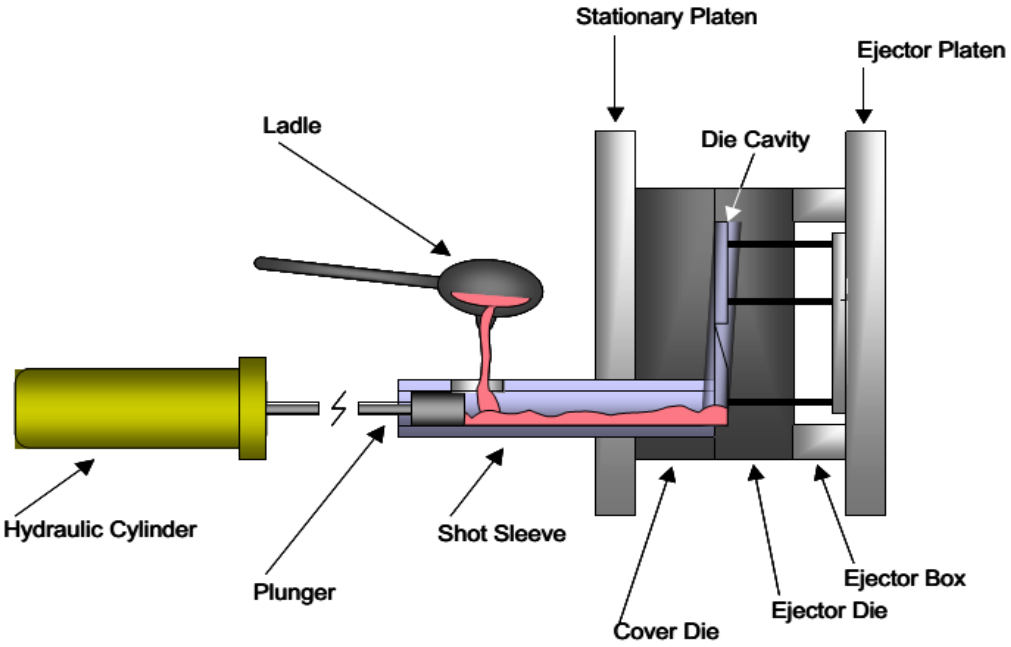

Fig. 3. Schematic of cold chamber die casting. [46]

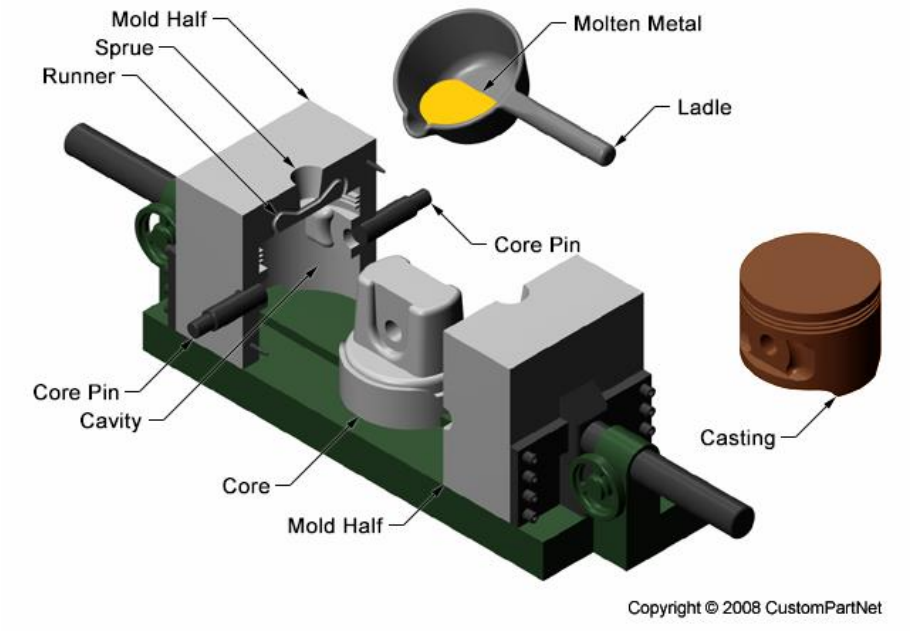

Fig. 4. Schematic of permanent mold casting [48]

2.2.4 As-cast microstructures

A schematic representation of variation of microstructural characteristics of Mg cast alloys has been illustrated in Fig. 5. The change in grain size is evident from the figure as the cooling rate increases; finer grains are observed with faster cooler rates and vice versa. Porosity, interdentritic zone and eutectic phases are shown. The cells that are adjacent to each other and of the same orientation are collectively known as a grain.

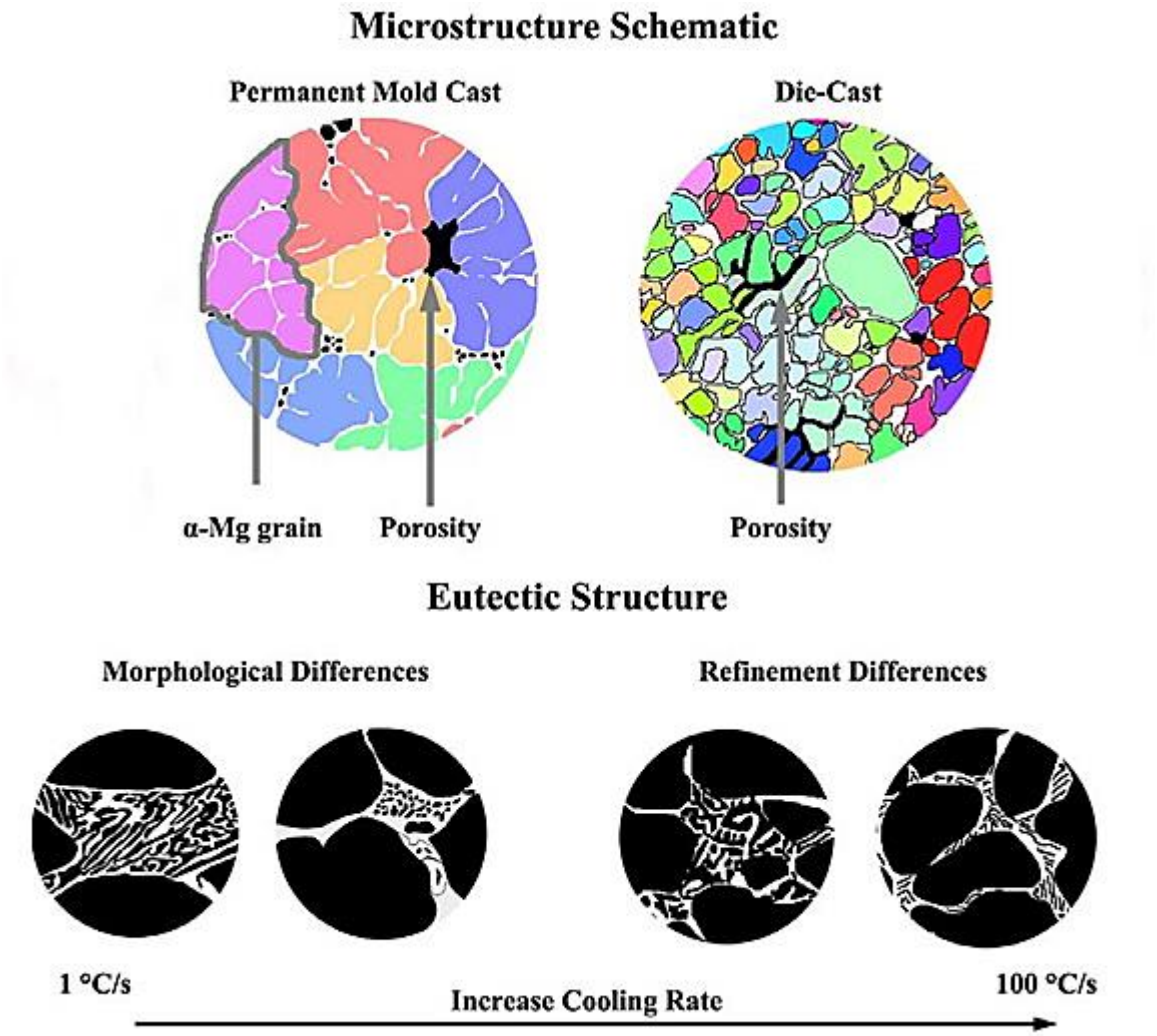

Fig. 5. Schematic illustration of Mg alloy solidification process and microstructure.

Understanding the interrelationship between processing routes, chemistry, microstructure, and mechanical behaviour is vital for optimizing the resultant properties. This investigation will utilize both permanent mold cast samples and high pressure die cast samples to study the influence of composition on microstructure and creep behaviour of MRI230D alloy. Permanent mold casting was selected for its attractive costs, intermediate cooling rate and availability when compared to die-casting. However, the die casting methosd is the popular one among smaller size component manufacturers [49].

2.3 Creep

Creep can be defined as the plastic deformation methodology that occurs at raised temperatures, majorly above half of the melting point. It is a time dependent deformation phenomenon. Fig. 6 shows an example of a typical creep curve for metals, creep strain vs. time. Creep strain is a function of stress, time and temperature [50]. Creep deformation comprises of three stages namely, primary, secondary and tertiary respectively. Primary creep shows decreased creep rate due to work hardening is dominating to that of recover (softening). Secondary stage finds a balance between the same and tertiary shows greater creep strain owing to necking, resulting in fracture.

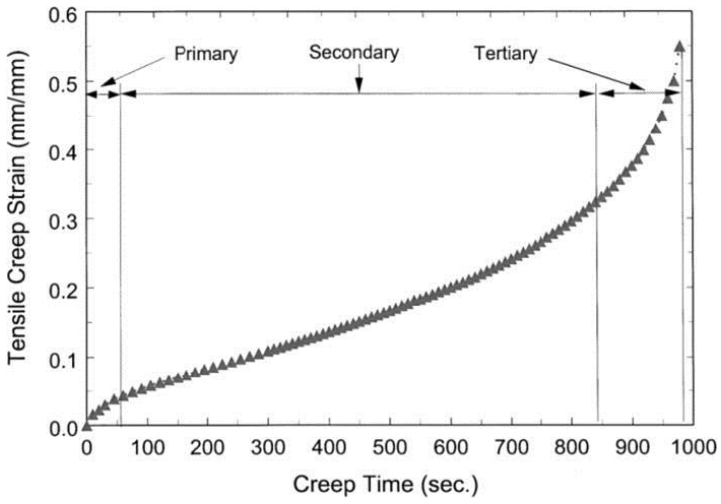

Fig. 6. Shows a typical creep curve for metals, strain vs. time.[51]

Creep deformation may be classified mainly into three distinct paths that arise at the microscopic level. They are;

1. Dislocation creep
2. Diffusion creep
3. Grain boundary sliding (GBS)

These mechanisms may occur during deformation individually as well as simultaneously. [52-54]. The determining factors of the mechanisms are temperature, stress level and grain size.

2.3.1 Dislocation creep

The relative change of position of dislocations in the interior of grain lattice in the course of deformation which consists of both glide and climb coordinated creep is called Dislocation creep. The glide along the slip planes are referred to as Glide-controlled creep .This creep routine arises chiefly due to the hindrance of dislocation movement by solute atoms [63,64]. Characteristic stress exponent 'n' measured in the corresponding alloys are accurate about 3. The creep rate equation was given by [53]:

$$\dot{\varepsilon} = K D_S \sigma^3$$

where D_s is the diffusion coefficient of the solute atom in the alloy.

Climb-controlled creep as the name denotes is the climbing up of dislocations across hindrances with the loss of energy. This classification of dislocation creep is more difficult occurs for elemental metals and their corresponding alloys. The characteristic value of stress exponent n is typically about 4-5. The creep rate equation can be expressed by [65]:

$$\dot{\varepsilon} = K D_L \sigma^n$$

where D_L is the lattice diffusion coefficient.

2.3.2 Diffusional creep

Matter when being transported from one region to another by the virtue of temperature hence facilitating deformation is referred as Diffusional creep. He occurrence generally happens at temperatures close to 0.9 T_m in fine grained materials [53]. Diffusional creep is categorised into Nabarro-Herring creep and Coble creep. The mechanism Nabarro-Herring creep is behind Lattice diffusion in movement of matter, while grain boundary diffusion is the culprit behind Coble creep. Grain size is a matter of prime importance for Coble creep when compared to Nabarro-Hering creep. In addition, the activation energy for Nabarro-Herring creep is larger than that for Coble creep [66].

2.3.3 Grain Boundary Sliding (GBS)

Working at elevated temperatures the grains within a polycrystalline metal are often forced to change positions relative to each other. Stress level (strain rate) and temperatures are two deciding factors for this movement. Grain boundary sliding is essentially the commonest occurring creep deformation regime for superplastic flow. The grains slide past each other and may end up with a differential shapes in this mechanism. GBS is often followed by a complementary mechanism. Unless the GBS is followed by another of the two remaining mechanisms, failure due to premature fracture shall follow at the triple points.[53, 55, 56, 57]. Fig. 7 is a model established by Fukuyo [58] based on GBS followed by slip which involves the sequential steps of glide and climb.

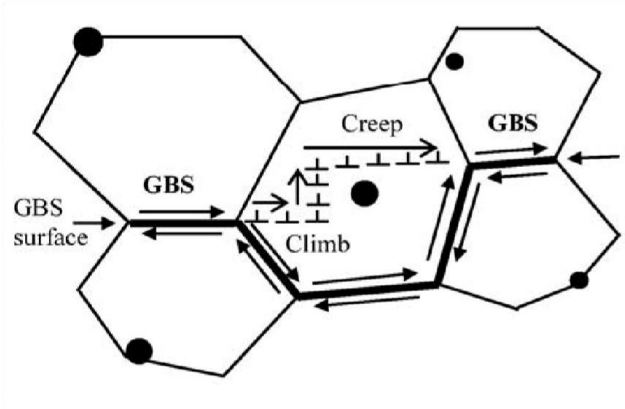

Fig 7. A model based on a Grain Boundary Sliding process[58].

The activation energy is either equal to lattice diffusion energy or grain boundary diffusion energy. Grain boundary sliding is more predominant in the fine grained structure, when compared to the coarse grain structure. The value of the exponent of stress 'n' should be in the range of 2-3 for the GBS to take place. GBS is a plastic flow mechanism that contains dislocation glide and dislocation climb by which the movement of dislocation take place. GBS showed major contribution to overall strain for other fine-grained superplastic alloys as well [59-62]. GBS is more predominant in fine grained material.

2.3.4 Deformation mechanism maps

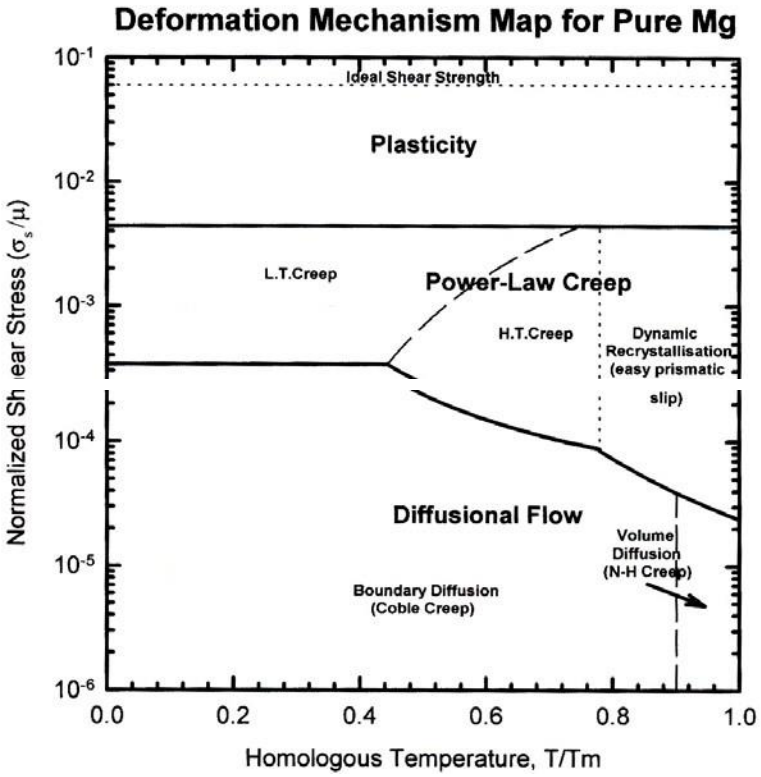

Fig. 8. Shows the standard deformation mechanism map.[67]

Ashby [68] established graphs that could predict the deformation mechanism with models. The plots were established to determine the deformation mechanisms upon a given alloy/system, grain size, load and homologous temperature. Frost and Ashby [67] published literature of several deformation maps and the magnesium map is shown in Fig. 8.

2.4 Variation of creep properties with casting conditions

Comparisons between the creep behaviour of various Mg alloy have been conducted to understand the correlation between microstructure and creep characteristics. The apt casting technology is one of the important decisions taken by the manufacturers especially when they intend to go on large scale production as that in automobiles and electronics. Following are some of the relevant works which led to the idea of the thesis.

Gutman et al. (1997) [69] studied the dependence of casting parameters of permanent mold casting and die casting on creep behaviour of AZ91D. It was found out that the alloy density affected the creep behaviour appreciably. In addition, the permanent mold cast alloy showcased improvement in creep resistance due the precipitation of intermetallics with lesser mould temperature. However, the die cast alloy performance was found to be dependent on the degree of micro and macro porosity. Caceres et al. (2002) [70] investigated the effects of solidification rate and ageing on microstructural properties of AZ91 alloy. They found out that the dendrite arm spacing, SDAS, decreased considerably with the decreasing solidification time with the Mg-Al-Zn system. The comparison was held between sand casting and high pressure die casting. Moreover, they probed into the strengthening mechanisms like grain boundary strengthening, solid solution hardening and dispersion strengthening.

Zhu et al. (2008) [71] reported the creep properties of MRI153M alloy in various casting conditions, ingot-cast, di-cast and squeeze cast technologies respectively. The squeeze cast material reported the highest creep property and the die-cast specimen reported the lowest. The authors suggested that the inferior creep resistance of the fine grained die-cast was due to the grain boundary sliding and maximized porosity among all. The squeeze cast alloy scored above the ingot-cast in creep resistance owing to the strengthening of the secondary eutectic particles inhibiting dislocation movement at the grain boundaries. Han et al. (2009) [13] reported the refinement of microstructure and nanoscale indentation creep behaviour of Mg-Al-Ca alloys. Cooling rates ranging from 0.5 to 65◦C/s were conducted and properties were found to be superior for the alloy casted from 20°C/s. SEM micrographs showcased rapidly solidified systems having superior grain refinement on the permanent mold AC52 alloy. Nanoscale indentation creep deformation resistance improved for fast cooling alloys that demonstrated combined strength of solid solution strengthening and dispersion strengthening.

Zheng et al. (2010) [72] studied the microstructure and creep behaviour of Mg–3Sm–0.5Zn–0.4Zr (wt.%) produced by different casting technologies. Dislocation creep was found to be the predominant rate determining mechanism at a stress level of 60MPa and 200°C. Die-cast alloy exhibited superior creep behaviour owing to the dynamically precipitated platelets that are fine, hindering dislocation movement. The regions of highly supersaturated solid solubility were absent in the case of ingot casting. Ferri et al. [12] solidified Mg–Al–Ca–La under varied heat extraction routines. The fast cooling rates displayed greater refinement in microstructure and better mechanical properties as in the case of die-casting. This paper studies the ZAXLa05413 magnesium alloy, figure out the relationship between solidification parameters and mechanical properties.

Bai et al. (2012) [73] investigated microstructure and creep behaviour of Mg–4Al–(1–4) La produced by various casting techniques, permanent mold casting and die-casting respectively. Al was found to exist in three different forms other than the solute atoms. HPDC alloy displayed superior creep characteristics with La amount more than 2% from the presence of dense network of Al11La3 phase along the dendrite boundaries. Besides the solidification rate, the pressure applied while solidification is also taken into account for the superior performance of HPDC alloys. Xu et al. [74] reported considered permanent mold casting and direct chill casting of extruded Mg–Al–Ca–Mn alloy for microstructural and mechanical property determination. The die cast alloy retained a lamellar eutectic structure and refined dendrite cell size when compared to that of permanent mold casting. Kim et al. [14] examined ATX421 alloy produced by die-cast and ingot cast conditions. They saw the die-cast alloy exhibiting greater tensile and yield strength at 200°C and room temperature. The high cooling rate resulted in regions of super saturation of solid solution near the interdentritic boundaries for the die cast alloy unlike the ingot-cast alloy. The die cast alloy showcased finer, larger volume fraction and thin intermetallic phases when compared to that of the ingot-cast. The dispersion strengthening effect was clearly understood by the pinning of dislocation movement and preventing grain boundary sliding during the test. Chen et al. (2013) [75] examined Mg–6Zn–3Sn–2Al–0.2Ca alloy fabricated by water-cooling mold casting under pressure. They tried out casting with various cooling rates and characterized die cast with fine grain size, appreciably distributed secondary phases and small dendrite arm spacing. The mechanical properties were also testified. Horie, et al. [76], reviewed the creep performance of die cast and permanent mold cast Mg - 2Zn - 0.8Ca – 2 RE (rare earth mischmetal) – 0.5Zr, temperature range of 120–180°C at stress regime of 40 to 100 MPa. The die-cast samples

displayed decreased thermal stability, while reported an increase in creep resistance by a factor of 10 over the permanent mold cast samples. The stress exponent for the die-cast alloy calculated was greater than seven. Fine precipitates within the α-Mg grains were testified and it was established they play a vital role in improving the tensile properties and creep deformation of Mg-Zn-Ca-RE-Zr alloys.

CHAPTER 3: EXPERIMENTAL PROCEDURE

The chemical composition of the MRI230D alloy as reported in [19].

3.1 Casting specifications

The HPDC alloy was cast into cylindrical rods of diameter 19 mm and 179 mm length by means of a cold chamber high pressure die-casting machine. The IC alloy cast into a rectangular casting with dimension of 350mmX125mmX60mm from gravity casting (permanent mold casting).

3.2 XRD analysis

In order to study the phases present in the specimen, X-ray diffraction (PANalytical model: DY-1656) was done using CuKα (λ=1.5418A°) radiation. The scanning range used for the diffraction was 10°- 90° with a step size of 2°/min.

3.3 Optical microscopy (OM) and Scanning electron microscopy (SEM)

Optical micrographs were taken. The microstructure was characterized by scanning electron microscope (JEOL 6480 LV), equipped with an energy dispersive X-ray spectroscopy (EDS) for chemical composition analysis of phases present. The specimens for microstructural study were made by typical metallographic techniques. Etching was conducted with a solution of 100 ml ethanol, 10 ml acetic acid, 6 ml picric acid and 20 ml of distilled water. Microstructures were observed in the as-cast and after creep conditions.

3.4 Creep tests

The multiple specimens for compressive creep tests were made of 6 mm diameter and 15 mm length, cut out from the castings by spark erosion. All the creep tests were conducted in using a lever arm (10:1) creep machine (Model: ATS 2330) .The stress range employed in the present investigation was of the range 60 to 120 MPa and at temperatures of 175ºC and 200ºC.

CHAPTER 4: RESULTS AND DISCUSSION

4.1 As-cast microstructure

Fig. 9 illustrates the XRD patterns attained from the as-cast HPDC and IC specimen of the MRI230D respectively. It is obvious from the pattern that the alloy in both die-cast and ingot-cast condition comprises of primary α-Mg(Mg) peak and the peak matching to $(Mg,Al)_2Ca$ phase. One of the most important findings was the absence of β-phase ($Mg_{17}Al_{12}$) that has relatively lower thermal stability and melting point. The addition of Ca led to the complete suppression of β-$Mg_{17}Al_{12}$ which is valuable for elevated temperature properties. Mondal et al. [77] testified the exclusion of β phase in a Mg-Al alloy adding RE as alloying element. Bai et al. [73] too reported the repression of β phase in both die-cast and ingot-cast Mg-4Al-(1-4)La alloy.

Optical microstructure images of the MRI230D alloy fabricated by various casting technologies, HPDC and IC technologies respectively, are shown in Fig. 10 (a&b). Evidently the alloy in both casting conditions comprises of polygon grains. Nevertheless, it is clear that the HPDC alloy revealed comparatively finer grain size to that of the IC alloy.The grains in the HPDC specimen are dense and the grain boundary network are closely arranged confirming significant room temperature properties. Total average grain size concluded by linear intercept method, 35±1 μm and 8±0.5 μm for both the alloys, respectively. The difference in grain size was due to the considerable variation in cooling rate of the HPDC and IC technologies. Ingot cast has a lower solidification rate of about 10-20°C/s, while high pressure die cast acquires several hundred degrees per sec.

The SEM images, secondary electron scattered micrographs of the MRI230D alloy in various casting technologies are revealed in Fig. 11 (a&b) (both 1000x for representation) and the enlarged view of Fig. 11(b) is presented in Fig. 11(c). EDS analysis performed along the interior part of the grain is demonstrated in Fig. 11(c) and showcased an average chemical division of 96.50±0.67 Mg, 2.70±0.64 Al, 0.30±0.14 Ca, 0.19±0.05 Sr, 0.17±0.03 Sn and

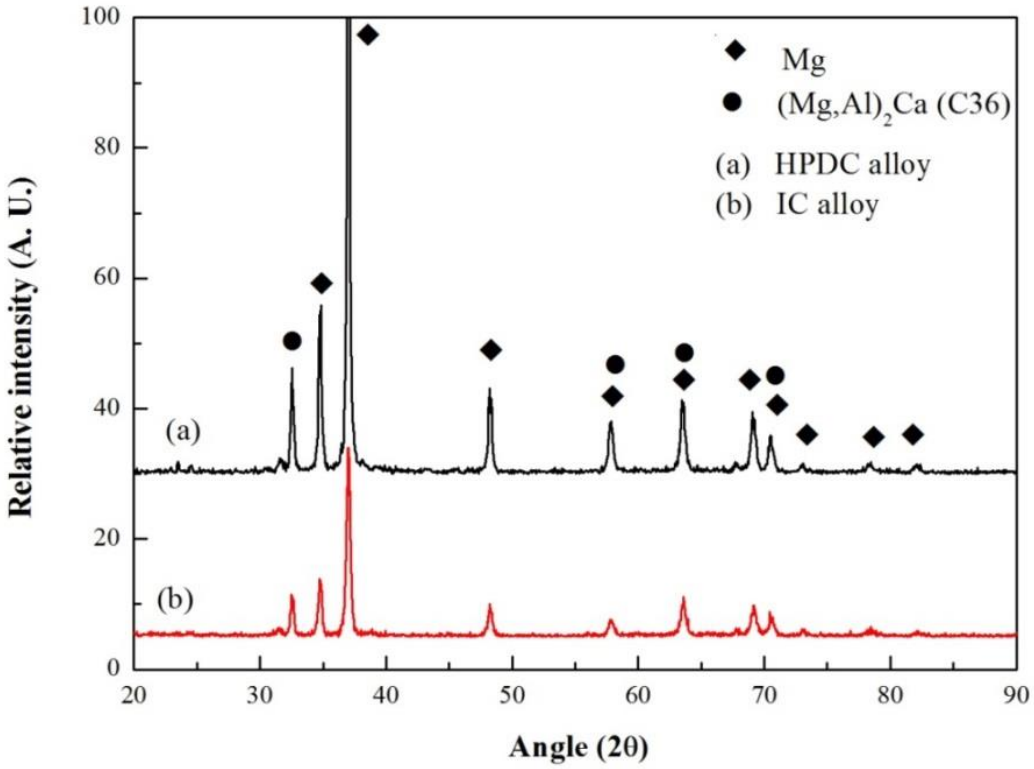

Fig. 9. XRD patterns from the ingot-cast and die-cast specimens.

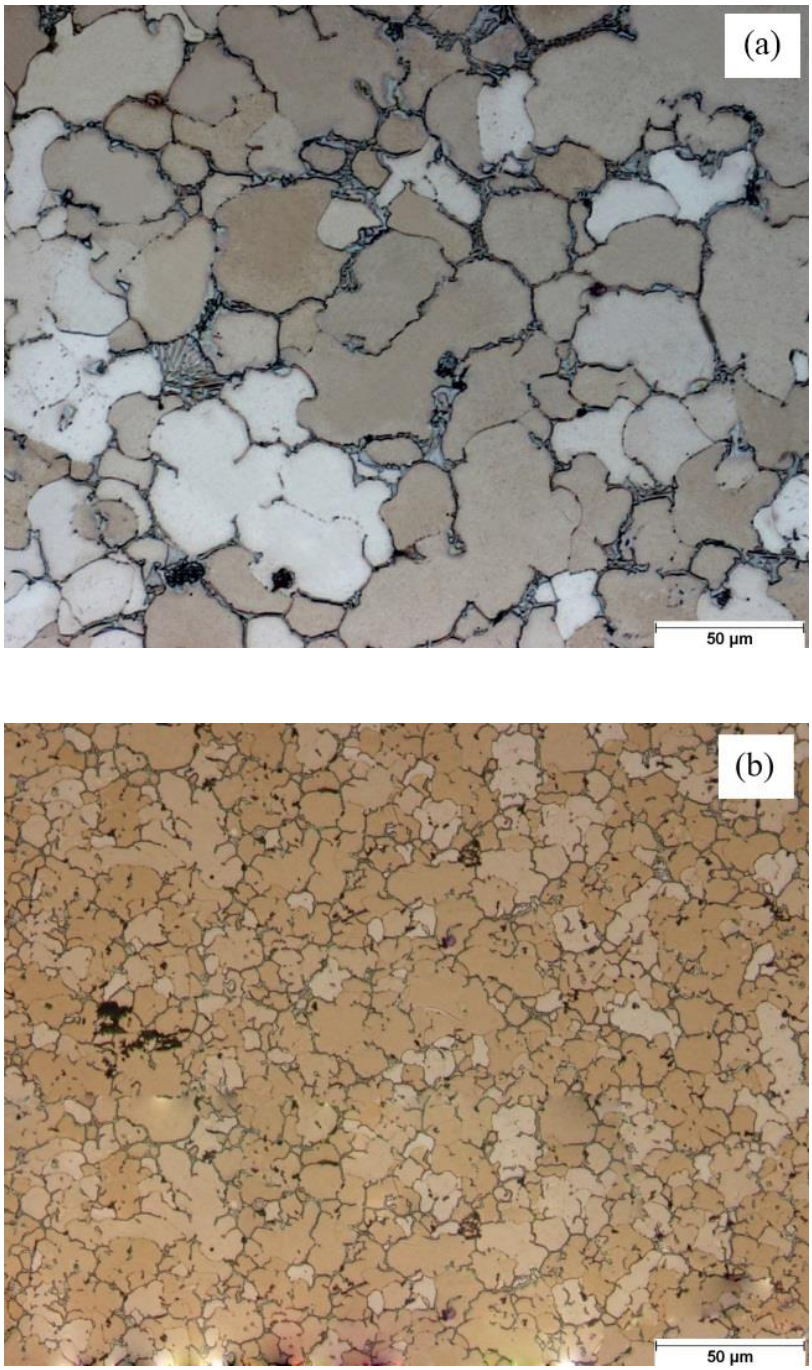

Fig. 10. Optical images of the alloy fabricated by (a) IC and (b) HPDC process.

0.20±0.06 Mn (at.%), that represents α-Mg. Likewise, EDS analysis obtained along the lamellar phases obtained across the interdentritic region (grain boundary) and triple points reported a total average composition of 38.7±4.2 Mg, 45.2±7.3 Al and 15.8±1.8 Ca (at.%). Terada et al. [78] carried out an EDS analysis along the grain boundaries of the secondary phase and observed the composition of 24.7 Mg, 56.9 Al and 18.0 Ca (at.%) . They testified the phase as C36 ($(Mg, Al)_2Ca$) in the corresponding litertaure. Hence, we are forced to conclude that the grain boundary phase may possibly be the C36 phase as represented with arrows pointed towards in Fig. 11(c). Moreover, an Al-Mn rich phase (represented with arrows in Fig. 11(c)) were also detected and the corresponding EDS analysis demonstrated a total average chemical composition of 52.3±8.6 Al, 39.6±2.3 Mn and 8.1±0.8 Mg (at.%). EDS representation was also obtained upon the IC specimen (noticeable from arrows in Fig. 11(a)) similar phases. Hence, the MRI230D Mg alloy in both casting conditions approves the existence of identical phases i.e., α-Mg, C36 and Al-Mn rich phase.

The IC and HPDC specimens exhibited noticeable variation in their microstructural characteristics. Most evident differentiating factor was the finer grain size of the HPDC specimen. The cooling rate of IC alloys prepared from permanent mold gravity cast alloys are in the scale of 10-20ºC/s and that of the cold chamber high pressure die cast alloys are 100-120ºC/s, respectively [74]. The excessive degree of undercooling correlated with the speedier solidification rate following HPDC enables the formation of a larger number of nuclei in the liquid alloy matrix. Nevertheless, the poor diffusion rate at the subsequent temperature lead to low growth rate resulting in grain refinement [79]. In addition, the volume fraction of secondary eutectic phases (C36) saw an appreciable change, clearly distinguishable from Fig. 3 (a and c). The change in C36 volume fraction was quantitatively analyzed (average) to be 9.1±0.4% and 12.8±3.2% respectively for the IC and HPDC specimens. Higher the cooling rate higher would be the deviation of solidus line from the equilibrium condition. Hence, faster cooling rate enables the HPDC specimen to have a large amount of eutectic phases and a small amount of solutes (essentialy Al) in solid solution.

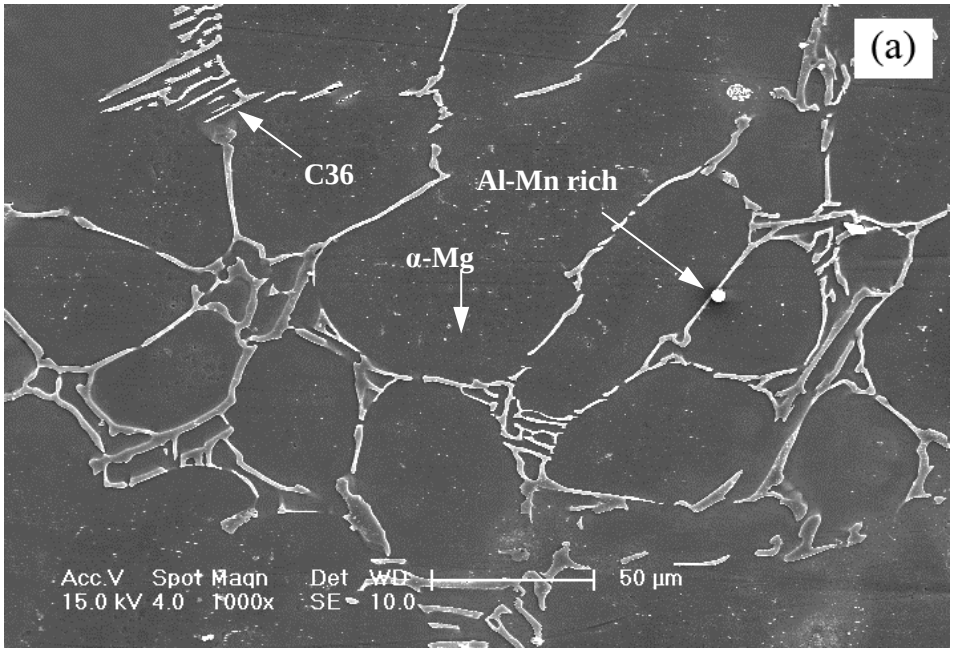
(a)
C36
Al-Mn rich
α-Mg
Acc.V Spot Magn Det WD 50 µm
15.0 kV 4.0 1000x SE 10.0

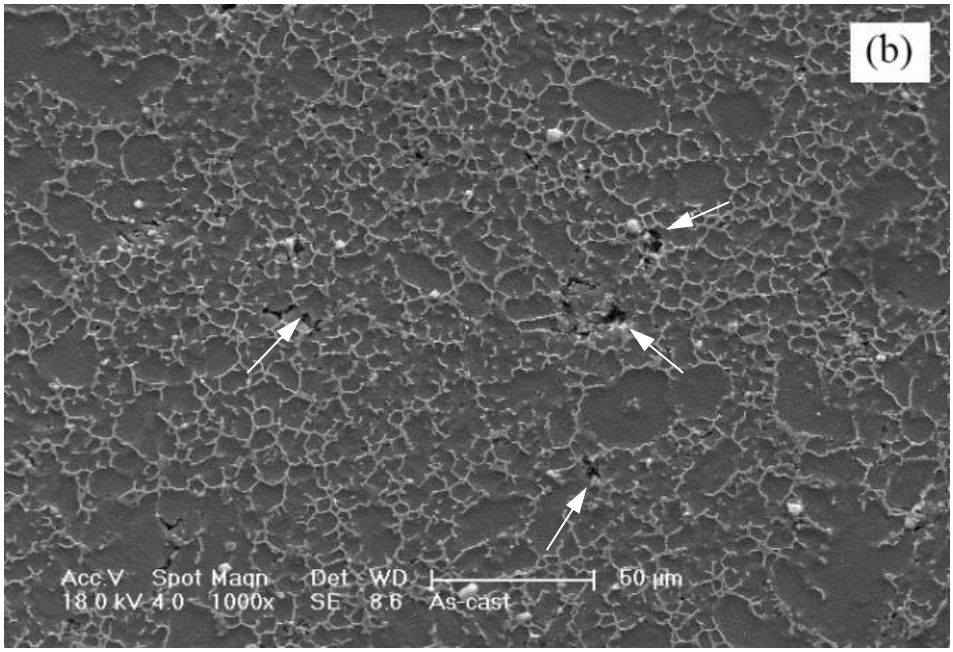
(b)
Acc.V Spot Magn Det WD 50 µm
18.0 kV 4.0 1000x SE 8.6 As-cast

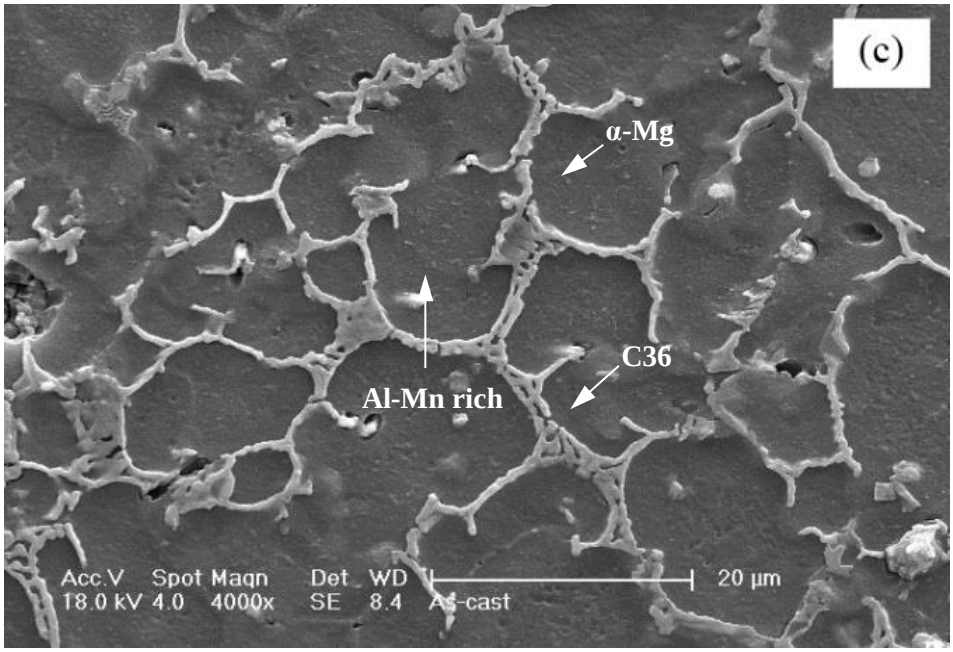

Fig. 11. SEM images in (a) IC, (b) HPDC process and (c) magnified view of (b).

Han et al. [13] detected that the computed volume fraction of the grain boundary phase improved with increase in solidification rate in the AC52 alloy. Moreover, the morphology of the eutectic phases differed owing again to the solidification time. The secondary eutectic C36 percipitates were found to be coarser in the IC specimen, Fig. 3(a) and Fig. 3(c), while the HPDC alloy potrayed finer and dense network of C36 precipitates by the grain boundaries and the triple points due to the sudden cooling. The IC alloy allowed adequate time for enlargement of the precipitates, hence broadening the lamellar structure of the secondary phase. Therefore, fine and highly oriented dendrites are formed by fast cooling, while large and coarse dendrites are generated by slow cooling.

Porosity is another noteworthy distinction among the two alloys produced from HPDC and IC technologies. Appreciable extent of pososity was exhibited by the HPDC specimen when compared to that of the minimal measure in the IC specimen. They are shown in Fig. 11(b) with arrows. The excessive porosity detected in the HPDC alloy was credited to the dissimilarity in liquid melt temperature, air entrapment during pressurizing with casting conditions that includes the process of preperation of the melt and mould temperature[80].

Additionally, dissimilarity in the amount of pressure applied during solidification among the two casting technologies employed in the present study may also influence the microstructure of both the castings. The greater pressure in HPDC alloy could bring about finer grains with finer secondary eutectic phases.

4.3 Creep characteristics

Typical strain vs. time creep plots of the MRI230D alloy produced by high pressure die casting and ingot casting conditions at a constant stress of 70 MPa for 50h, temperature regime of 175°C and 200°C are shown in Fig. 12. The varied solidification rates saw altered creep characteristics on both the alloys. Since all the tests were done under compression and 50 hour was the time limit, the plots are well short of attaining the tertiary stage. All strain rates were calculated from the secondary state region of the strain vs. time plots. Fig. 13 shows the quantitative strain rates of each creep test indicated in Fig. 12, the respective creep rates are calculated based on the linear straight line fit method. From Fig. 12, clearly the IC alloy demonstrated greater creep deformation to that of the HPDC alloy at both 175°C and 200°C at 70 MPa tested for 50 hours. It is striking that at 200°C IC specimen exhibited relatively larger creep deformation when compared to all other regimes.

The HPDC alloy displayed a strain rate of 1.74×10^{-8} s^{-1}, 175°C and it was increased to 5.35×10^{-8} s^{-1} at 200°C. Thus the creep rate raised by a factor equal to 3.1. Likewise, the IC alloy demonstrated a strain rate of 3.92×10^{-8} s^{-1} at 175°C which was intensified to 1.28×10^{-7} s^{-1} at 200°C. Therefore, the creep rate increased by a factor of 3.3. The IC alloy exhibited a larger jump in terms of the extent of decrease in creep deformation resistance at elevated temperatures. Another significant remark was the factor of difference of creep rates of both the specimens at a particular temperature and 70 MPa stress level, they were found to be similar. For instance, at 175°C, the ratio of creep rates of IC to HPDC, ie. 3.92×10^{-8} s^{-1} to 1.74×10^{-8} s^{-1} is 2.25. Likewise, at 200°C, the creep rates of IC and HPDC are 1.28×10^{-7} s^{-1} and 5.35×10^{-8} s^{1}. They gave a factor of 2.35, which is not so deviant from 2.25. Therefore, creep deformation of both the alloys produced by two different casting conditions did not vary significantly till 200°C. This observation may not hold good for even higher temperatures.

Additionally, compression creep test at 200°C and 70MPa was performed thrice on the HPDC to check the reproducibility of the creep rate, shown in Fig. 14(a).The creep rates calculated at the steady state region by linear straight line fit method of Fig. 14(a) is shown in Fig. 14(b). The creep rates were 6.30×10^{-8} s^{-1}, 5.35×10^{-8} s^{-1} and 5.79×10^{-8} s^{-1} agreeing to first, second and third run, respectively. The observed creep rates were precise enough to be declared as reproducible since they differ by a factor from 1.1 to 1.8 with respect to each other. Mondal et al. [77] reported a creep rate of 5.30×10^{-8} s^{-1} under similar test conditions, which is in harmony with the current investigation of HPDC specimen at 200°C and 70MPa (i.e.,5.35×10^{-8} s^{-1}). Zheng et al. [72] and Kim et al. [14] too stated mediocre creep deformation resistance of the IC alloy as compared to the HPDC alloy, while Zhu et al. [71] reported superior creep behaviour for the IC alloy. Furthermore, the ratio of creep rates (i.e., $\acute{\varepsilon}_{IC}/\acute{\varepsilon}_{HPDC}$ equal to 2.25) in the present study is well in harmony with that observation from Zheng et al. [72] and Kim et al. [14] with the unlike the higher value reported by Zhu et al. [71] of 2.14, 3.24 and 0.13 respectively.

Additionally, dependency of stress value on the creep rate was investigated at 175°C and 200°C in double logarithmic scale for the present alloy produced by both casting technologies, shown in Fig. 15.

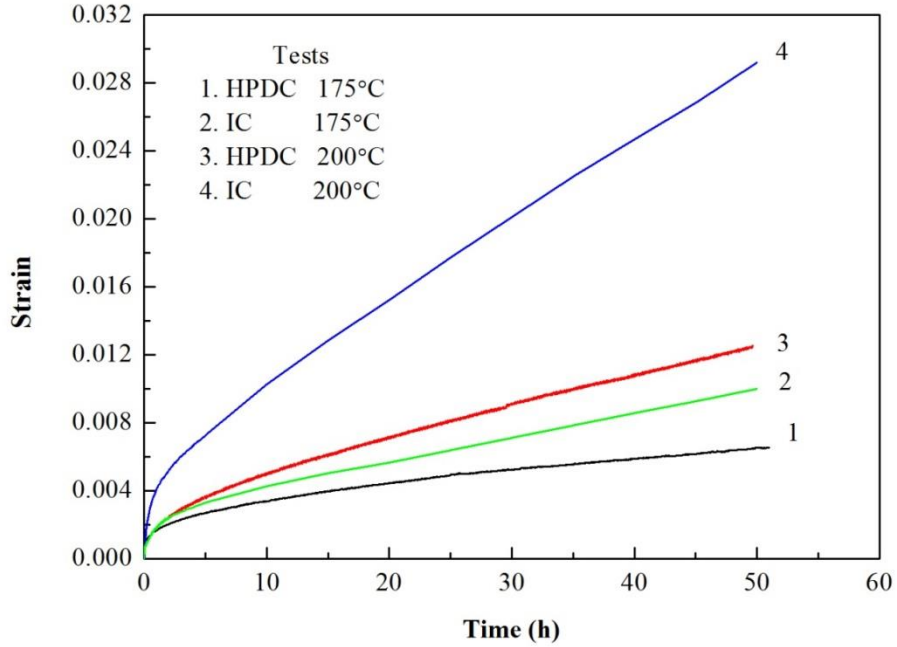

Fig. 12. Typical creep curves (Strain vs. time) of MRI230D alloy, for the IC and HPDC process, tested for 50h with 70 MPa stress and at temperature of 175°C and 200°C.

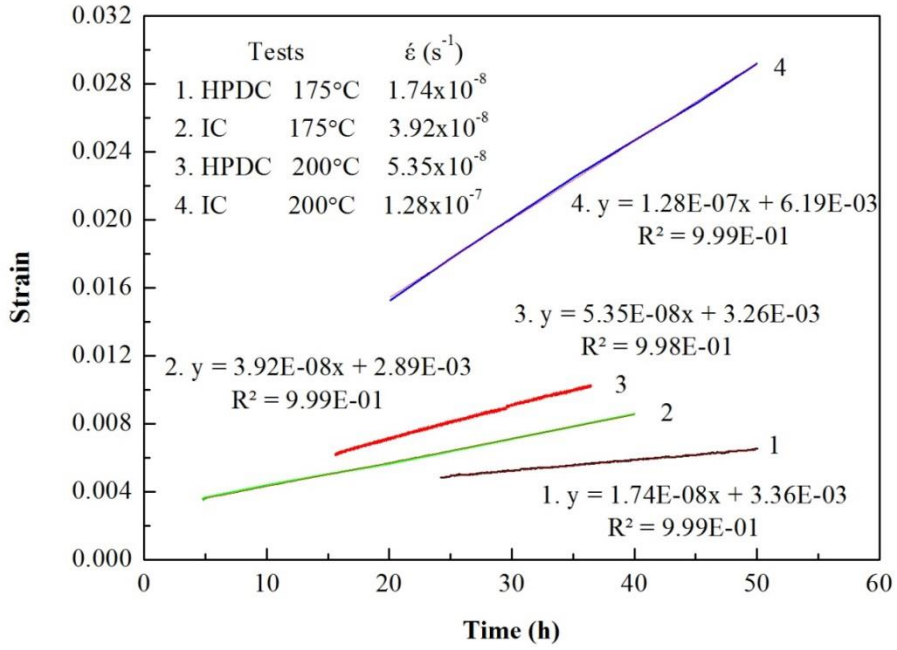

Fig. 13. Strain rate plots computed with straight line fit method from shown in Fig.4.

(a)

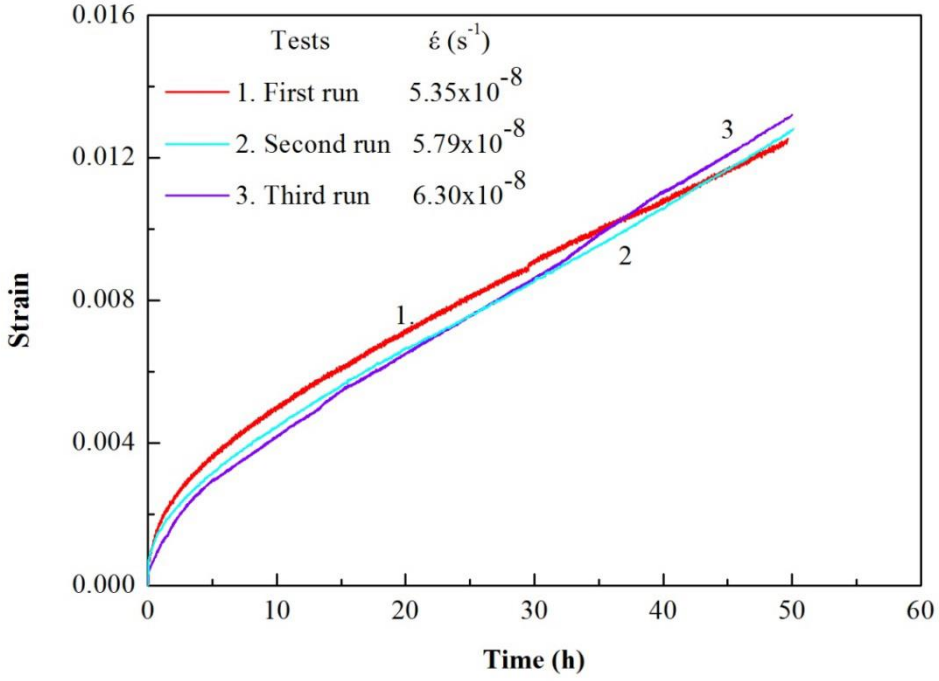

(b)

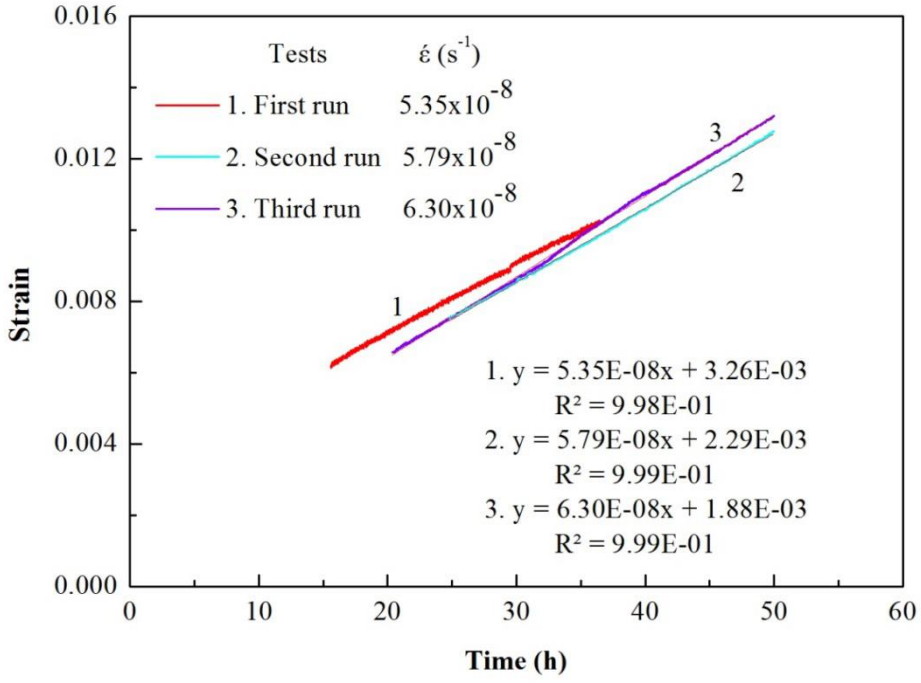

Fig. 14.(a) Strain vs. time graphs representative of three runs and (b) computation of strain rate by linear straight line fit to the plots presented in (a) for the HPDC MRI230D alloy creep tested for 50h, stress of 70 MPa and 200°C.

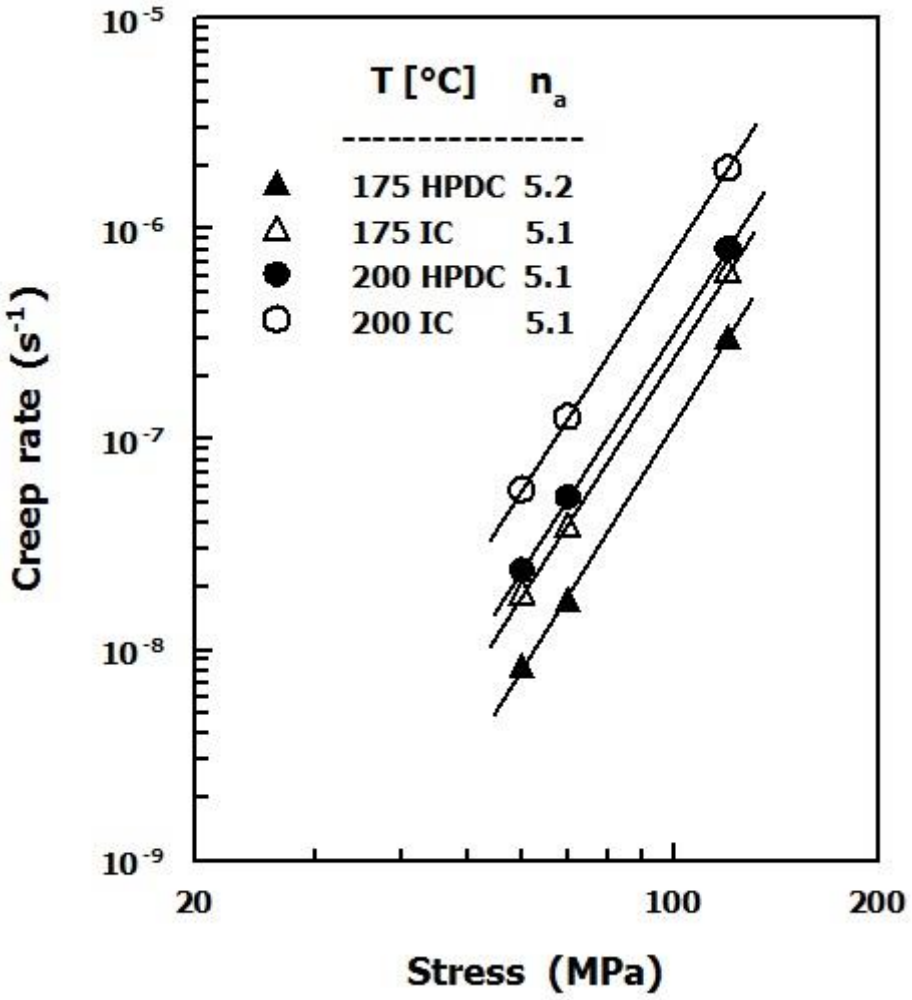

Fig. 15. The stress dependency of creep rate for HPDC alloy.

The stress exponent, n_a, was calculated using fitting straight line to the strain rates obtained at 60MPa, 70MPa and 120MPa at temperatures 175°C and 200°C respectively. In the present investigation, the value of stress exponents obtained were 5.1and 5.2 revealing that the deformation governing creep mechanism was dislocation climb in both the alloys [63,64,81]. Dieringa et al. [82] the obtained stress exponents with MRI230D that matches with those values reported in the present investigation. The apparent activation energy, Q_c, could not be measured considering the lack of data. Terada et al. [83] also settled with the conclusion that the rate controlling methodology in the AX52 alloy is dislocation creep. Dislocation climb was stated as the governing creep mechanism in Mg alloys [84-86].

The deformation mechanism in the present investigation of HPDC and IC alloys was reassured to be dislocation creep by theoretically determining the normalized stress (σ/G) and homologous temperature (T/T_m). Accordingly, spotting the region corresponding to the values in the deformation mechanism map established for Mg alloy [87]. The value of Young's modulus (E) of the alloy was taken as 45 GPa [34] and the poisson's ratio for metals were assumed as 0.33 so as to attain the magnitude of shear modulus (G) to be 32.14 GPa. As a result, $2.0*10^{-3}$ was achieved as the ratio for σ/G, which is positioned in the theoretical range of dislocation creep (i.e., $10^{-4} < (\sigma/G) < 10^{-2}$) [88]. The magnitudes of (T/T_m) were 0.48 and 0.51 at 175°C and 200°C, respectively. The data point's which correspond to individual combinations of (σ/G) and (T/T_m) were observed and was confirmed that they lie within the theoretical area of dislocation creep in the deformation mechanism map established for Mg alloys [87].

4.4 Microstructural changes after creep tests

The SEM images of the MRI230D alloys cast under HPDC and IC conditions experienced 50 h of creep test at a stress of 70 MPa and temperature routine of 200ºC is shown in Fig. 16 (a&b). The only significant change observed in the microstructures of the creep tested specimens of both alloys as compared to the as-cast microstructures was the nature and the amount of phase present along the grain boundaries and the triple points. It was noticed that in both IC and HPDC alloys after 50 h of creep test the volume of existing secondary eutectic C36 phase was increased. The α-Mg grain boundaries saw fresh precipitation of eutectic C36 phase where the Al supersaturation was dominant before undergoing the creep tests. The C36 intermetallic phase which is thermally stable up to 500ºC (773K) due to its higher melting temperature and reported to be favourable for creep resistance [27,34]. As a result, the stable

C36 phase chiefly supports the creep deformation resistance of the alloy cast using both the conditions. In addition, there was no proof of formation of any new phase in the alloy during creep tests at 175ºC or 200ºC. Maximum amount C36 phase was detected in the HPDC specimens, as the total amount of pre-existent C36 phase was larger. Earlier, Mondal et al. [77] reported an enhancement in C36 phase after creep tests with same alloy. Another striking fact from the literature was the transformation of C36 phase into C15 (Al_2Ca) phase in the Mg–5.0Al–3.0Ca (wt.%) alloy after getting exposed to heating at 300ºC for 100 h [33]. Nevertheless, the period and the temperature exercised in the current study are lesser and hence, no change was seen in the C36 phase after the creep tests. The same nature was also detected in the alloys following creep tests for 50h at a stress of 70 MPa and 175ºC.

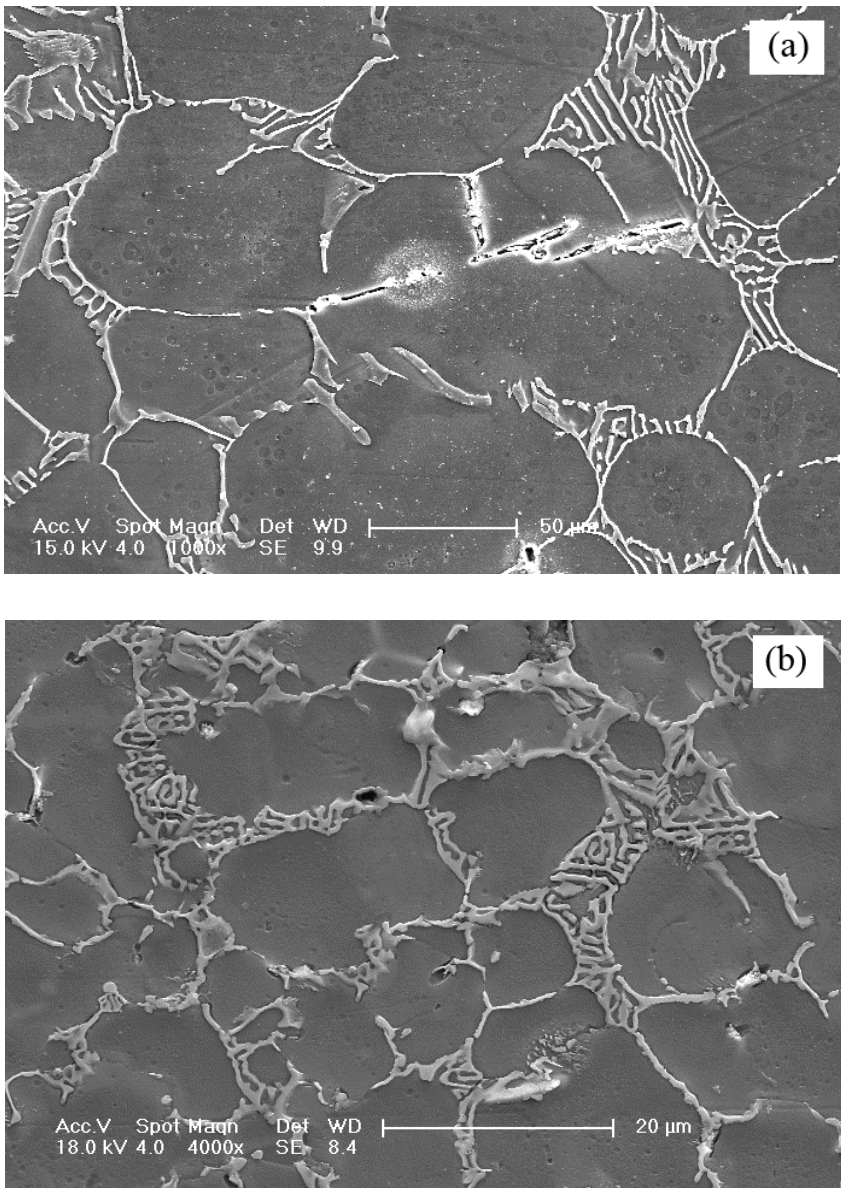

Fig. 16. SEM micrographs of the MRI230D alloys after creep test for 50 h at 70 MPa stress and temperature of 200°C corresponding to (a) IC alloy and (b) HPDC alloy.

4.5 Reasons behind difference in creep behaviour

The as-cast micrographs are largely non-homogeneous along with casting conditions that are far-off from equilibrium cooling. Therefore, the microstructural characteristics take responsibility of the dissimilar creep behaviour. Dislocation creep was stated as the predominant creep deformation mechanism in the current study. Clearly, when creep deformation is being controlled by movement of dislocations, any hindrance to dislocation glide/climb propagation on basal or non-basal planes are anticipated to improve the resistance to creep. Finer grain size was exhibited by the HPDC alloy promising superior room temperature properties. On the contrary, grain size takes a trivial role in the creep resistance when the chief mechanism of deformation is dislocation creep. The single most important reason of the superior creep deformation resistance offered by the HPDC alloy was the fine and dense network eutectic secondary phase present along the grain boundaries/interdentritic zones and triple points. The thermally stable (upto 500°C /773K) C36 phase found dispersed in the α-Mg matrix pinned dislocation movements largely. Consequently, the IC alloy having lowered volume fraction of C36 phase would easily deform at elevated temperature in comparison owing to the inferior dispersion strengthening effect. Moreover, the coarser IC alloy eutectic secondary phases possess moderate pinning effect when compared to the closely spaced phases in the HPDC alloy, adding on to the creep resistance. Zheng et al. [72] stated that the fairly-distributed precipitates have substantial ability to impede dislocation motion on basal plane. Kim et al. reported that the coarse C36 phase forced to initiate cracks and thus permitted dislocation movement [14].

The greater extent of porosity detected in HPDC alloy affected undesirably on the creep behaviour of MRI230D alloy in the present investigation. Gutman et al. [69,80] reported that in HPDC alloy, the extent of creep is determined by the degree of porosity present in the alloy. They suggested that in an identical test specification, the minimum creep rate mostly increases with an increase in porosity. Nevertheless, the negative effect of the existence of porosity in the creep characteristics of the HPDC alloy in the current investigation was possibly insignificant (although not calculated) since there are much superior factors that adds on to the creep resistance.

CHAPTER 5: CONCLUSION

The correlation between the as-cast microstructure and creep behaviour of the MRI230D Mg alloy produced by two different casting technologies (i.e., ingot-casting (IC) and high pressure die-casting (HPDC)) were investigated. A detailed microstructural characterization and the evaluation of mechanical properties have been carried out. Following are the conclusions ascending from the present investigation.

1. The HPDC alloy demonstrated comparatively smaller grain size, finer and dense network of the secondary phase of higher volume fraction in contrast to the IC alloy. The amount of porosity was greater in the HPDC alloy.
2. Significant creep resistance was demonstrated by the HPDC alloy than the IC alloy with all the stress routines and temperature schemes in the current investigation.
3. The superior creep resistance of the HPDC alloy was chiefly indebted to the fine and dense network of the eutectic C36 phase which is of higher volume fraction, existing alongside the grain boundaries and triple points in α-Mg matrix impeding dislocation movement in the course of creep deformation.
4. The extent of enhancement of eutectic C36 phase in both alloys post creep tests varied and was appreciable in the HPDC alloy, which is favourable for creep resistance.

REFERENCES

[1] A.A. Luo, JOM 54 (2002) 42.

[2] G.V. Raynor, The Physical Metallurgy of Magnesium and Its Alloys, Pergamon Press, London-New York-Paris-Los Angeles, 1959.

[3] M.S. Dargusch, G.L. Dunlop, K. Pettersen, in: B.L. Mordike, K.U. Kainer (Eds.), Magnesium Alloys and Their Applications, Werkstoff-Informationsgesellschaft, Frankfurt, 1998, pp. 277-282.

[4] A.A. Luo, Int. Mater. Rev. 49 (2004) 13-30.

[5] M.O. Pekguleryuz, A.A. Kaya, Adv. Eng. Mater. 5 (2004) 866-878.

[6] Q.D. Wang, W.Z. Chen, X.Q. Zeng, Y.Z. Lu, W.J. Ding, Y.P. Zhu, X.P. Xu, J. Mater. Sci. 36 (2001) 3035-3040.

[7] S.S. Li, B. Tang, D.B. Zeng, J. Alloys Compd. 437 (2007) 317-321.

[8] E. Aghion, B. Bronfin, F.V. Buch, S. Schumann, H. Friedrich, JOM 55 (2003) 30-33.

[9] S.M. Zhu, B.L. Mordike, J.F. Nie, Mater. Sci. Eng. A 483-484 (2008) 583-586.

[10] C.J. Bettles, C.T. Forwood, D.H. StJohn, M.T. Frost, D.S. Jones, M. Qian, G.L. Song, J.R. Griffiths, J.F. Nie, Magnesium Technology 2003, ed. H.I. Kaplan, (TMS, Warrendale, PA, 2003), pp. 223-226.

[11] S. Spigarelli, M. Regev, E. Evangelista, A. Rosen, Mater. Sci. Tech. 17 (2001) 627-638.

[12] T.V. Ferri, A.P. Figueiredo, C.R.F. Ferreira, W. Hormaza, C.A. Santos, J.A. Spim, Mater. Sci. Eng. A 527 (2010) 4624-4632.

[13] L. Han, D.O. Northwood, X. Nie, H. Hu, Mater. Sci. Eng. A 512 (2009) 58-66.

[14] B.H. Kim, S.M. Jo, Y.C. Lee, Y.H. Park, I.M. Park, Mater. Sci. Eng. A 535 (2012) 40-47.

[15] H.E Friedrich, B.L. Mordike, eds. Magnesium Technology- Metallurgy, Design Data, Applications, Springer, Berlin, 2006, pp. 665.

[16] Weast, R.C., ed. Handbook of Chemistry and Physics, 57th ed, CRC Press, Cleveland, 1976.

[17] Sutton, L.E., ed. Table of interatomic distances and configuration in molecules and ions, Chemical Society London, Vol. 18, 1965.

[18] Magnesium Electron Limited, Magnesium alloy database, MATUS Databases, Engineering Information Co. Ltd, 1992.

[19] J.R. TerBush, J.W. Jones, T.M. Pollock, in: M.O. Pekguleryuz, N.R. Neelameggham, R.S. Beals, E.A. Nyberg (Eds.), Magnesium Technology 2008, TMS, Warrendale

(PA, USA), 2008, pp. 117–122.

[20] J.A. Hines, R.C. McCune, J.E. Allison, B.R. Powell, L. Ouimet, W.L. Miller, R. Beals, L. Kopka, P.P. Ried, SAE Technical Paper, Warrendale, Pa: SAE, 2006, No.2006-01-0522.

[21] Q. Jin, J.P. Eom, S. Lim, W.W. Park, B.S. You, Scr. Mater., 49 (2003) 1129.

[22] E.F.Em1ey, Principle of Magnesium Technology, Pergamon press, First edition, 1966, 925.

[23] P. L. Schaffer, Y. C. Lee, A. K. Dahle, Proc. Magnesium Technology 2001, J. Hryn ed., The Minerals, Metals and Materials Society, pp.81.

[24] A.A. Luo, T. Shinoda, SAE Technical Paper No.980086, Warrendale, Pa: SAE, 1998, 117.

[25] K.Y. Sohn, J.W. Jones, J.E. Allison, Magnesium Technology 2000, ed. H.I. Kaplan, J. Hryn, B. Clow, TMS, Warrendale, PA, 2000, 271278.

[26] K.Y. Sohn, J.W. Jones, J. Berkmortel, H. Hu, and J.E. Allison, SAE, Warrendale, PA: SAE, 2000, No.2000-01-1120.

[27] A.A. Luo, M.P. Balogh, B.R. Powell, Metall. Mater. Trans. A 33 (2002) 567-573.

[28] A.A.. Luo, M.P. Balogh, and B.R. Powell, SAE Technical Paper No.2001-01-0423, Warrendale, Pa: SAE, 2001, 118

[29] B.R. Powell, A.A. Luo, V. Rezhets, J. Bommarito, B.L. Tiwari, SAE Technical Paper No.2001-01-0422, Warrendale, Pa: SAE, 2001, 120.

[30] Terada, N. Ishimatsu, R. Sota, T. Sato, K. Ohori, Mater. Sci. Forum, 2003, 419-422, p. 459-464.

[31] M. Pekguleryuz , J. Renaud, Magnesium Technology 2000, ed. H. Kaplan, J. Hryn, ,B. Clow,Warrendale, PA, 2000, 279-284.

[32] A. Suzuki , N.D. Saddock, J.W. Jones, and T.M. Pollock, Scripta Mater., 2004 51(10) 1005-1010.

[33] A. Suzuki, N.D. Saddock, J.W. Jones, T.M. Pollock, Acta Mater. 53 (2005) 2823-2834.

[34] A. Suzuki, N.D. Saddock, J.W. Jones, T.M. Pollock, Metall. Mater. Trans. A 37 (2006) 975-983.

[35] A. Suzuki, N.D. Saddock, J.R. TerBush, B.R. Powell, J.W. Jones, and T.M. Pollock, Magnesium Technology 2007, ed. R. Beals, TMS, Warrendale, PA, 2007.

[36] T. Horie, H. Iwahori, Y. Seno, Y. Awano, Magnesium Technology 2000, ed. H.I. Kaplan, J. Hryn, B. Clow, TMS, Warrendale, PA, 2000, 261-269.

[37] N.D. Saddock, A. Suzuki, J.R. TerBush, T.M. Pollock, and J.W. Jones, Magnesium Technology 2007, ed. R. Beals, TMS, Warrendale, PA, 2007, 407-412.

[38] M.O. Pekguleryuz, J. Renaud, Magnesium Technology 2000, ed. H.I. Kaplan, J. Hryn, and B. Clow, TMS, Warrendale, Pa, 2000, 279-284.

[39] K. Ozturk, Y. Zhong, A.A. Lou, Z.K. Liu, JOM, 2003 55(11) 40-44.

[40] E.Aghion, B. Bronfin, F.V. Buch, S. Schumann, and H. Friedrich, Magnesium Technology 2003, ed. H.I. Kaplan, (TMS, Warrendale, PA, 2003), 177-182.

[41] C. Mendis, L. Bourgeois, B. Muddle, and J.F. Nie, Magnesium Technology 2003, ed. H.I. Kaplan, TMS, Warrendale, PA, 2003, 183-188.

[42] Y. Terada, N. Ishimatsu, Y. Mori, T. Sato, Mater. Trans., 46(2) (2005) 145-147.

[43] Last accessed on http://www.dsmag.co.il/?cmd=products.5&act=read&id=2

[44] H. Friedrich, S. Schumann, J Mater Proc Tech, 117 (2001) 276 .

[45] E.J. Vinarcik, High Integrity Die Casting Processes, John Wiley & Sons, Inc., New York, NY, 2003.

[46] A.A. Alan, Journal of Magnesium and Alloys, 1 (2013) 2-22.

[47] M. Nehan, R. Maloney, SAE Paper No. 960419, Warrendale, PA, (1996).

[48] Last accessed on http://www.custompartnet.com/wu/die-casting

[49] A. Luo and M. O. Pekguleryuz, Journal of Materials Science, 29 (1994) 5259.

[50] Introduction to Creep: R. W. Evans and B. Wilshire: The Institute of Materials, London, 1993, p19.

[51] Y. Lee, Journal of Electronic Packaging, ASME copyright 133 (2011) 044501.

[52] H. Somekawa, Mater. Sci. Eng. A, 407 (2005) 53.

[53] T. G. Nieh, J. Wadsworth, O. D. Sherby, Superplasticity in Metals and Ceramics, Cambridge England, New York, NY, USA: Cambridge University Press, 1997.

[54] O. D. Sherby and J. Wadsworth, Prog. Mater Sci. 33 (1989)169-210.

[55] T. Mohri, M. Mabuchi, M. Nakamura, T. Asahina, H. Iwasaki, T. Aizawa, K. Higashi, Mater. Sci. Eng. A 290 (2000) 139-144.

[56] Y. Takigawa, J. V. Aguirre, E. M. Taleff, K. Higashi, Mater. Sci. Eng. A. 497 (2008) 139-146.

[57] R. Panicker, A. H. Chokshi, R. K. Mishra, R. Verma, P. E. Krajewski, Acta Mater.(2009) 57 3683-3690.

[58] H. Fukuyo, H.C. Tsai, T.Oyama, O.D.Sherby, ISIJ International 31 (1991) 76-85.

[59] O. A. K. R.Z. Valiev, Acta. Metall. 31(1983) 2121.

[60] K. Matsuki, N. Hariyama, M. Tokizawa, Y. Murakami, Met. Sci. 17 (1983) 503.

[61] T.G. Langdon, J. Mater. Sci. 16 (1981) 2613.

[62] R. C. Gifkins, Mater. Forum 15 (1991) 82.

[63] O.D. Sherby, P.M. Burke, Prog. Mater. Sci. 13 (1968) 325-390.

[64] J. Weertman, J. Appl. Phys. 28(1957) 1185-1191.

[65] J. Weertman, Transactions of the ASM, 61 (1968) 681-694.

[66] F.R.N. Nabarro, Philosophical Magazine. A, 16 (1967) 231-237.

[67] H.J. Frost, M.F. Ashby, Deformation-Mechanism Maps - The Plasticity and Creep of Metals and Ceramics. 1982 Pergamon Press. 166.

[68] M.F. Ashby, Acta. Metall. , 20(7) (1972) 887-897.

[69] E.M. Gutman, Ya. Unigovski, M. Levkovich, Z. Koren , E. Aghion, M. Dangur, Mater. Sci. Eng. A 234-236 (1997) 880-883.

[70] C.H. Caceres, C.J. Davidson, J.R. Griffiths, C.L. Newton, Mater. Sci. Eng. A 325 (2002) 344-355.

[71] S.M. Zhu, B.L. Mordike, J.F. Nie, Mater. Sci. Eng. A 483-484 (2008) 583-586.

[72] J. Zheng, Q. Wang, Z. Jin, T. Peng, J. Alloys Compd. 496 (2010) 351-356.

[73] J. Bai, Y. Sun, F. Xue, J. Qiang, Mater. Sci. Eng. A 552 (2012) 472-480.

[74] S.W. Xu, K. Oh-ishi, S. Kamado, F. Uchida, T. Homma, K. Hono, Scripta Mater. 65 (2011) 269-272.

[75] Chen Jihua, Wei Juying, Yan Hongge, Su Bin, Pan Xueqiang , Mater. Des. 45 (2013) 300–307.

[76] Horie, T., H. Iwahori, Y. Seno, and Y. Awano, Magnesium Technology 2000, ed. H.I. Kaplan, J. Hryn, and B. Clow, TMS, Warrendale, PA, 2000, 261-269.

[77] A.K. Mondal, D. Fechner, S. Kumar, H. Dieringa, P. Maier, K.U. Kainer, Mater. Sci. Eng. A 527 (2010) 2289-2296.

[78] Y. Terada, R. Sata, N. Ishimatsu, T. Sato, K. Ohori, Metall. Mater. Trans. A 35 (2004) 3029-3032.

[79] E.J. Lavernia, T.S. Srivatsan, J. Mater. Sci. 45 (2010) 287-325.

[80] E.M. Gutman, Y. Unigovski, M. Levkovitch, Z. Koren, J. Mater. Sci. Lett. 17 (1998) 1787-1789.

[81] F.A. Mohamed, T.G. Langdon, Acta. Metall. (1974) 22(6) 779-788.

[82] H. Dieringa, Y. Huang, P. Wittke, M. Klein, F. Walther, M. Dikovits, C. Poletti, Mater. Sci. Eng. A 585 (2013) 430-438

[83] Y. Terada, N. Ishimatsu, T. Sato, Mater. Trans. 48 (2007) 2329-2335.

[84] A. Arunachaleswaran, I.M. Pereira, H. Dieringa, Y. Huang, N. Hort, B.K. Dhindaw, Mater. Sci. Eng. A 460–461 (2007) 268-76.

[85] H. Dieringa, Y. Huang, P. Mainer, N. Hort, K.U. Kainer, Mater. Sci. Eng. A 410-411 (2005) 85-89.

[86] V. Sklenicka, T.G. Langdon, J. Mater. Sci. 39 (2004) 1647-1652

[87] M.F. Ashby, D.R.H. Jones, Engineering Materials I: An Introduction to Their Properties and Applications, second ed., Butterworth Heienemann, Netherland, 1996.

[88] G.E. Dieter, Mechanical Metallurgy, fourth ed., McGraw-Hill, London, 2000.